Tampere University

Antti Penttinen

SECOND-HARMONIC GENERATION OF SESAM Q-SWITCHED MICROCHIP LASERS

Faculty of Engineering and Natural Sciences
Master Thesis
May 2023

ABSTRACT

Antti Penttinen: Second-harmonic generation of SESAM Q-switched microchip lasers
Master Thesis
Tampere University
Masters Degree Program in Science and Engineering
May 2023

Pulsed laser sources are vital for a wide range of applications throughout the daily life. They are the key components in data transfer, medical use, industry as well as in variety of microscopic and spectroscopic applications. Novel microscopic and spectroscopic applications, such as photoacoustic microscopy or time-gated Raman spectroscopy require very specific pulsed laser sources. Even further, for many of these novel applications to reach a mature phase and foothold in our society, the light sources in use must come with affordable cost and compact footprint.

The optical properties required in many applications feature a combination of short pulses, high pulse repetition rates, high energies and suitable operation wavelengths. Many of these properties define the application measurement time or imaging depth and thus the right combination of these is vital.

For many novel applications requiring specific pulsed lasers, the options tend to be rather limited. Some solutions offer the required pulse repetition rates, enabling imaging speed and resolution, but are limited in pulse peak power, not generating imaging depth or targeted phenomena. Others can offer the correct optical parameters but the size or cost of such systems limits the applications. This issue of right combination of pulse parameters with a suitable technology platform was at the heart of this master thesis, with the focus on enabling novel imaging methods in the microscopic and spectroscopic applications.

This thesis focuses on the development of a compact microchip laser sources at 1534 nm with optical properties targeted for photoacoustic microscopy use. Lasers studied take advantage of a semiconductor saturable absorber mirrors (SESAM) technology to offer a unique combination of parameters with ns pulse duration, high repetition rate from tens of kHz to hundreds of kHz and kW pulse peak power. These lasers were frequency doubled to 767 nm using second harmonic generation in periodically poled lithium niobate (PPLN) to offer novel wavelength regions with suitable pulse parameters.

Keywords: LASER, SESAM, microchip, passive Q-switching, second-harmonic generation

TIIVISTELMÄ

Antti Penttinen: SESAM pohjaisten Q-kytkettyjen mikrosirulaserien taajuuskahdennus
Diplomityö
Tampereen yliopisto
Tekniikan ja luonnontieteiden diplomi insinööri
Toukokuu 2023

Pulssitetut laserit vaikuttavat jokapäiväisissä laitteissa nykymaailmassa. Niitä hyödynnetään tiedonsiirrossa, leikkausoperaatioissa, sekä useissa teollisuuden sovelluksissa. Niitä käytetään myös moderneissa spektroskopia ja mikroskopiasovelluksissa, joissa vaatimukset laserien kohdalla ovat paljon erityisemmät. Sovellusten yleistymiseen, lasereilta vaaditaan myös paljon enemmän kuin vain optisia ominaisuuksia. Niiden pitää olla kustannustehokkaita ja kannettavia, joka aiheuttaa omat haasteensa.

Monien pulssilasereita hyödyntävien sovellusten optisten ominaisuuksien vaatimuksiin kuuluvat lyhyt pulssin pituus, korkea pulssien toistotaajuus ja riittävä pulssienergia. Toistotaajuus vaikuttaa monesti mittausnopeuteenja -tarkkuuteen, kun taas ilman riittävää pulssienergiaa koko sovelluksen efekti voi jäädä havaitsematta. Näille sovelluksille sopivassa koossa toteutettu yhdistelmä oikeita pulssiparametreja olisi tarvittu ratkaisu ja voisi saada myös kaupallista kiinnostusta.

Useat nykyisistä laser ratkaisuista kykenee tarjoamaan osan optisista ominaisuuksista, mutta jää uupumaan joistain toisista. Toiset taas kykenevät tarjoamaan sopivat optiset ominaisuudet, mutta lasereiden koko tai hinta rajoittavat suuren määrän sovelluksia pois. Tämä työ keskittyi moderneihin spektroskopiasovelluksiin keskittyvän laser ratkaisun kehittämisessä, joka pystyisi vastaamaan kokonaisvaltaisiin laserille asetettuihin vaatimuksiin.

Diplomityö keskittyy puolijohdepeilillä toimivien mikrosirulasereiden kehittämiseen moderneihin spektroskopia ja mikroskopiasovelluksiin. Työn tavoitteena oli tutkia sopivaa laserkombinaatiota hyödyntämällä SESAM -puolijohdepeilirakenteita ja pienikokoista mikrosirulaseria. Kokeellinen osuus koostui sopivien pulssiominaisuuksien löytämisestä, sekä laserin aallonpituuskonversiosta tyyppillisesti haastavalle infrapuna aallonpituusalueen alkupuolelle.

Avainsanat: LASER, SESAM, microchip, passivinen Q-kytkentä, taajuuskahdennus

CONTENTS

1 INTRODUCTION

Many novel applications, such as time-gated Raman spectroscopy, photoacoustic microscopy (PAM) or Stimulated emission depletion (STED) microscopy are groundbreaking in their field of art, offering unique properties such as sub-diffraction limited resolution [1], real-time material analysis [2] or sub-tissue micrometer resolution images [3] to the end-user. All of these novel applications however require specific pulsed laser sources in the visible or near infrared range in order to bring out their benefits to the end user. Options for producing such pulsed lasing for these applications are limited due to their requirements on optical properties such as pulse duration, pulse repetition rate and pulse energy. Such applications in the fields of spectroscopy and imaging have strict requirements on the combination of high peak powers, good beam properties and sufficiently high repetition rates. Valid options for the light sources vary from semiconductor lasers to mode-locked lasers, but they all tend to have some drawbacks in terms of the comprehensive performance.

Semiconductor lasers can nowadays provide usable wavelengths in the visible to near infrared range by advancements in the GaN materials, but typically lack the peak power required in the above mentioned applications.[4] Otherwise the semiconductor lasers could create a viable option for many of such applications in the future due to their small size and low cost. Solid-state lasers on the other hand can offer sufficient energies but typically operate in the infrared region, namely 1 µm or 1.5 µm wavelength region and thus are directly not the solution in these cases. They are also often optically pumped and the availability of pump lasers limits the wavelengths to the typical regions.

One suitable option would be to use nonlinear conversion to allow for additional wavelengths, beyond the primitive operation frequencies. Second-harmonic generation with solid-state lasers, transforming the fundamental infrared operation frequency into the visible or near visible range. The need for pulsed laser source raises another question on how the pulsing should be formed. Viable options for these applications are limited to mode-locking and Q-switching due to the power limitations of pulsed semiconductor lasers.

Mode-locking is a pulsing form where different longitudinal laser modes are circulated around the laser cavity forming very short pulses with high repetition rates typically ranging from tens of MHz up to GHz. [5] Due to the short pulse durations and extremely high pulse repetition rates, these systems don't naturally support high energy pulses at 100-200 kHz and require expensive amplifiers to increase the energy and pulse pickers

to bring down the pulse repetition rate. [6] For example in photoacoustic microscopy the repetition rate goes beyond the maximum pulse repetition rate allowed by the detection system [7] and the mode-locked laser could not be of use as such. These additional requirements make mode-locked lasers rather complicated, ending up with too bulky and expensive for many applications.

Another traditional method of pulse forming is Q-switching, where the laser properties are modified to first store and then release energy in high energetic pulses. [8] By Q-switching, repetition rates from single pulses to tens of kilohertz have been typically available. These pulses can be in the sub-ns to ns pulse duration, which would be suitable for many of the applications and can provide pulse energies from µJ to mJ but is typically not suitable for operation in the hundreds of kilohertz pulse repetition rate. For many applications this is simply too low a repetition rate, limiting the measurement resolution or measurement time.

SESAM based Q-switching is a form of passive Q-switching, where a semiconductor saturable abrosber mirror (SESAM) is used as the passive Q-switching element. Pulsing mechanism is still Q-switching and thus high energy pulses can be formed. However, by using the semiconductor element for pulsing, the pulse repetition rate and pulse duration can be tuned to higher repetition rates up to MHz region and pulse durations to shorter than typically, down to 16 ps.[9] The positioning of SESAM Q-switching in comparison to mode-locking and traditional Q-switching is shown below in figure 1.1.

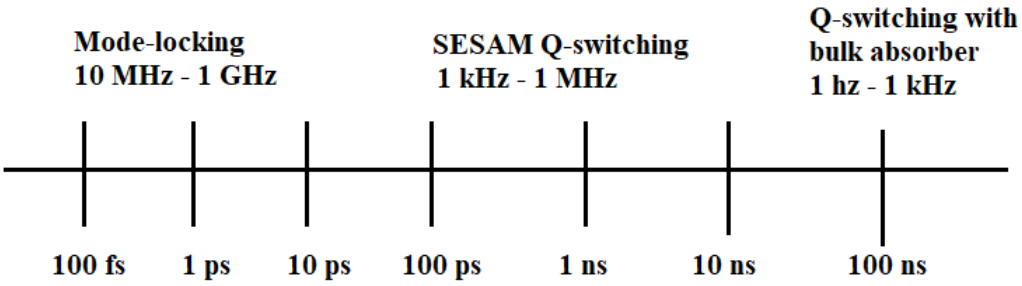

Figure 1.1. *Comparison of different pulsing method by pulse duration and pulse repetition rate. Modified from [10].*

Due to the good combination of pulsing parameters offered by the SESAM Q-switching and the clear benefits of nonlinear conversion to offer additional wavelengths, this combination was chosen as the technological approach of this thesis. By combining these two concepts with the methodology of compact microchip lasers, in which the laser cavity is formed between combined components a feasible study on generating optimal pulse parameters suitabls for novel microscopy and imaging applications.

Lasers were targeted to operate with pulse repetition rates between 10 - 100 kHz, offering

sufficient imaging resolution and imaging time. Pulse duration target was set in the ns region with peak powers ranging from hundreds of Watts up to Kilowatts. To extend the usability of the microchip lasers, wavelength conversion of these lasers into the near-IR region by second-harmonic generation was studied targetting combination of pulse parameters and operation wavelength hard to achieve by mature technologies.

The thesis will start from the theory of Q-switching, giving the focus on passive Q-switching and different saturable absorber options. A further outlook will continue to microchip lasers and moreover the SESAM Q-switched microchip lasers and extend to nonlinear conversion, covering the most typical forms of second and third order nonlinearities and the most often used nonlinear crystals. Lastly, the experimental work on the microchip seed lasers and the second harmonic generation will be covered, summarising the main results of the thesis.

2 THEORY OF Q-SWITCHING

In typical pulsed operation of lasers, such as pulsed semiconductor lasers, the upper limit of population inversion is restricted by simultaneous emission starting to eat away the upper state inversion at an early stage. Due to this, the amount of energy stored in the upper state of the gain material, never reaches an especially high amount and thus the pulses formed have a relatively low pulse energy. Q-switching is a method to change the cavity ability to lase thus allowing the system to gain much higher population inversion before lasing takes place. [8]

Laser cavity gain over losses per one roundtrip can be described by the cavity quality factor, also known as the Q–factor. Q–factor describes the laser cavity's ability to gain energy over the losses caused, meaning in case the Q–factor is very high, gain is much higher than losses over single roundtrip. But in case the Q–factor is very low, the losses over a roundtrip exceed the gain obtained. [5][10] Thus the Q–factor can be described as

$$Q = 2\pi \frac{2Lf}{c\alpha_{loss}}, \tag{2.1}$$

where L is the length of the cavity and f is the frequency of the laser, which combined describe the energy gained over a single length around the cavity. c is the speed of light and α_{loss} are the losses per cavity round trip. [8]

The principle of Q-switching is to allow the system to gain population inversion much higher than required for lasing by causing additional losses to the system. Once the energy has been stored, the additional losses can be removed and lasing can take place in the form of high energetic pulses. The procedure is called Q-switching, since the losses in the system are changed by switching the cavity Q-factor from high to low. Once a certain threshold has been achieved the Q-factor is switched to high value and pulse formation begins. [8][5] This process is described in figure 2.1 by Koechner.

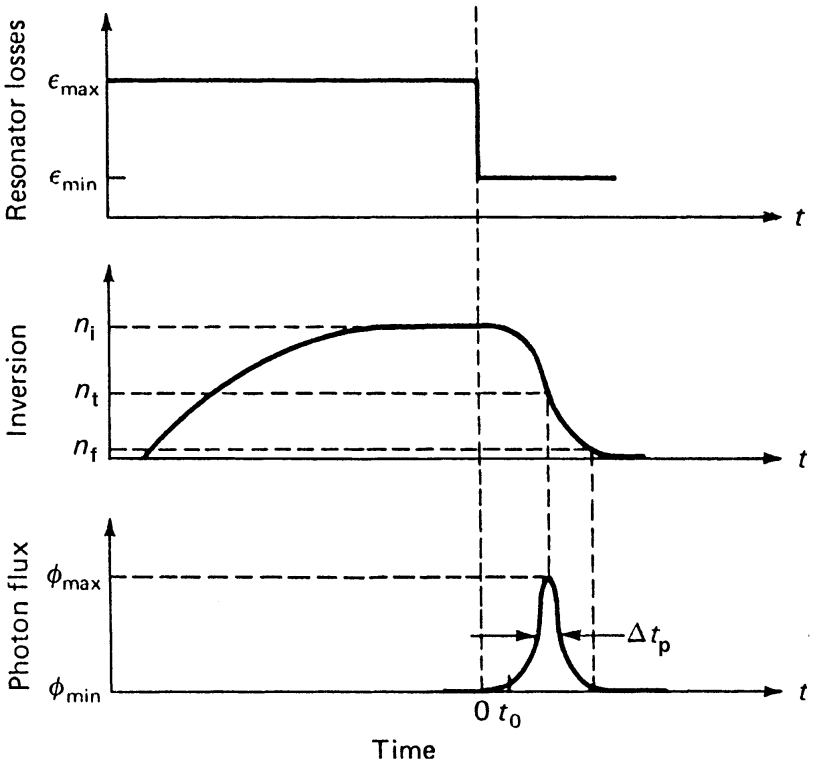

Figure 2.1. *Operation principle of pulse formation in Q-switching. Modified from [5].*

Figure 2.1 describes the three different factors influencing a Q-switching pulse formation. All three axis operate on the same timeline, the x-axis. In the beginning the resonator losses are kept at a high level to prevent lasing while population inversion is accumulated. Since the resonator losses are high, population inversion gains up but even though the threshold inversion n_t is passed in the figure up middle, the photon flux still remains at minimum level. This is the main difference of Q-switching to normal cw operation, where lasing would start to occur at n_t. In this case, the population inversion is increased and eventually saturates to n_i, until the resonator losses are changed, at time = 0 in figure 2.1. Once the losses are dropped, pulse forming starts

At a certain time point, namely at t=0 in the picture 2.1, the resonator losses are dropped and lasing may take place. Population inversion consequently drops down since the pulse formation begins. With rapid decrease in population inversion, the system is not able to support lasing for long and thus the laser pulse duration is kept very short.

Once the sequence has passed on for the first time, the resonator losses are increased back to a high value and lasing cannot take place. Population inversion starts to rise up again and after the next cycle the resonator losses can be dropped again for another laser pulse. The sequence of Q-switched lasing functionality is described by Nikkinen in picture 2.2.

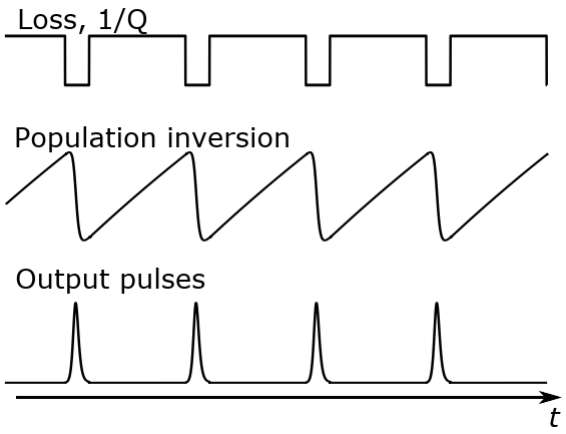

Figure 2.2. *Functionality of a Q-switched laser. Modified from [10].*

Due to the pulsing method of Q-switching, each pulse is formed independently from the others. This method has some benefits, such as reaching pulse repetition rates from few hertz up to MHz region and not having dependencies between the pulses. There are however also some disadvantages, for example, the fact that each pulse is formed independently causes intensity variations between the pulses as well as pulse-to-pulse timing jitter, which are natural to Q-switched lasers. In comparison, with mode-locked lasers the pulse repetition frequency is locked by the laser cavity, reducing timing jitter, where as with laser diodes the accumulation of inversion is at such a low level that delays between electronic pumping and optical output remain at very short time periods. [8]

The Q–switching cycle can either be externally activated or let to operate passively on its own. The two methods are namely called active and passive Q–switching. Active Q–switching includes methods such as mechanical Q–switches or electro-optical Q–switches, which allow for the tuning of cavity losses over time. In mechanical Q–switches the cavity Q–factor can be tuned by misaligning cavity mirrors or reducing reflectivity of the resonators. In the case of electro-optical switches, a very fast electronic shutters can be applied to change polarization of light within the cavity to prevent lasing before the Q-switching is preferred. [5] An example of an electro-optic Q-switch structure is presented by Koechner in figure 2.3.

While the actively Q-switched laser systems have some nice advantages, such as low timing jitter and high accuracy of the laser pulse emission, they also have some disadvantages. The systems are often bulky and large due to the components required for the Q-switching. Many of the systems require water cooling and complicated high-voltage driver electronics to operate the Q-switch. As reported by Koechner, the Q-switch needs to transit from high to low value in less than the laser build-up time. As an example for a very typical gain material, Nd: YAG, this means in a range of 150 - 200 ns. [5] This sets rather strict conditions to the Q-switch electronics, especially when the considering gain materials with shorter build-up time than Nd:YAG.

In comparison to active Q-switching, passive Q-switching goes through the pulsing cycle

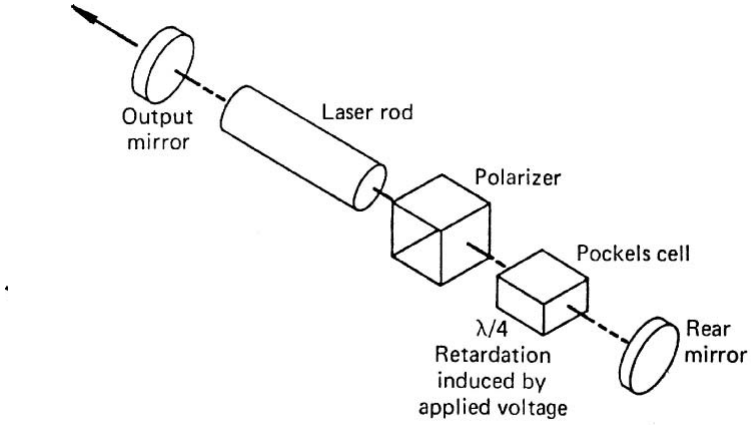

Figure 2.3. *Example structure of an electro-optic Q-switch. Modified from [5].*

on its own. This thesis will focus on passive Q-switching where the Q-switch and it's properties define the pulse characteristics without active control over the laser cavity. We'll discuss passive Q-switching, different Q-switch options and look into some of the passively Q-switched lasers.

2.1 Passive Q-switching

Due to the complexity of actively Q-switched devices, the branch of passive Q-switching is very popular method in pulse forming. In passive Q-switching the cavity losses are modulated by the nonlinear properties of the Q-switching element automatically. [8] Passively Q-switched lasers are thus much more simple, compact, robust and cost effective. However, they do not have equal precision of output pulse timing and have typically lower optical powers compared to the actively Q-switched lasers.[5]

Typical downsides of passive Q-switching include intensity variation and pulse-to-pulse timing jitter. Both of the artefacts are a consequence of passive pulse formation and typically occur in every passively Q-switched laser but their effect can be reduced. Intensity variation of the laser can be reduced by homogenising the Q-switch. In other words, in case the saturable absorber produces similar losses round after round, the system should work similarly overtime. Another very typical issue is the timing jitter between pulses. This effectively means that the pulsing frequency of the laser varies while the time between pulses does not remain constant. The effect comes as a consequence of the passive pulse forming, as no active element controls the exact pulse formation time.

For both of these artefacts the laser pumping can have a major impact. Especially when considering the timing jitter, great improvements can be achieved by using pulsed pumping instead of continuous wave pumping. In pulsed pumping, the optical pump is modulated by the pulse frequency, thus forcing the Q-switching to take place within certain pulse repetition rate. This method will limit the time within which the pulses can be emitted, also reducing timing jitter.

2.2 Saturable absorber

The passive Q–switch, called saturable absorber functions by initially absorbing the laser wavelength, causing additional losses to the cavity and thus preventing lasing. Saturable absorbers can be sformed of solid-state material, such as doped crystals or out of semiconductor materials. With solid-state absorbers, as the intensity on the absorber increases and the initial losses are saturated and the absorber eventually turns into a nearly transparent component, supporting the pulse formation [8][5] Figure 2.4 shows the nonlinear transmission behaviour of a typical, solid-state Q-switch in relation to the normalized saturation fluence of the absorber.

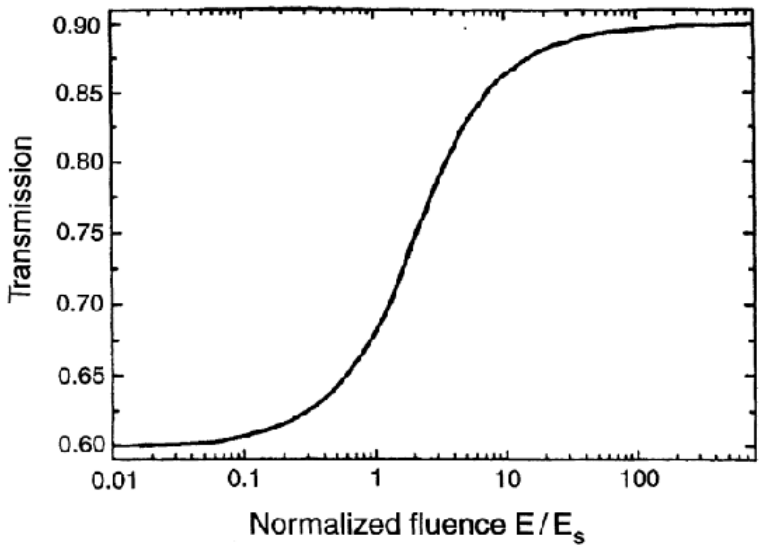

Figure 2.4. *Example of a nonlinear transmission of a saturable absorber, as a function of optical input fluence. [5].*

The initial transmission of the absorber starts here at approximately 60 %, preventing any lasing due to too high losses. As the spontaneous emission in the system increases, the losses start to dissipate as the Q-switch element saturates. Once the absorber has been saturated, the final transmission of 90 % allows lasing to take place and the Q-switched pulse is formed. [5]

The saturable absorber can be formed of a cell containing absorbing dye, gas, solid-state or semiconductor material. [8]. The first saturable absorbers were made of organic dyes, such as bis 4-dimethyl-aminodithiodibenzil-nickel (BDN) but the issue with dye absorbers was that they wore out over time and thus had very limited lifetime. Nowadays solid state absorbers, such as doped crystal materials, are much more popular. [5] These materials have improved thermal and mechanical properties providing extended lifetime and also easy operability due to solid-state structure. Such a saturable absorber operates like a three level energy diagram presented by Koechner in picture 2.5.

In such a material the transition from level 3 to 2 needs to be fast compared to transition between levels 2 and 1. The upper state lifetime on level 2 must also be long enough to

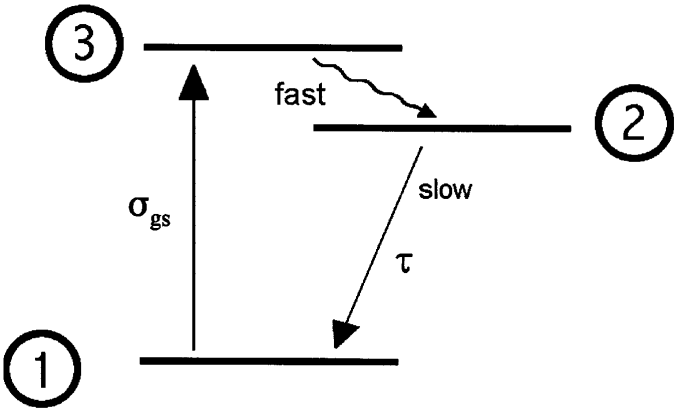

Figure 2.5. *Energy level diagram of a saturable absorber. Modified from [5].*

accumulate inversion and clear out the ground state. As the material absorbs light and fills the upper state, it starts to change its transmission according to figure 2.4. Once the population inversion is gained, absorber becomes practically transparent allowing lasing. [5] [8]

A very popular material for saturable absorber at 1 µm region is Cr^{4+}:YAG. The YAG crystal acts as a host for the Cr^{4+} ions with good thermo-optical and mechanical properties and is sufficiently easy to produce. The Cr^{4+} ions provide good absorption cross section for this wavelength region and are thus especially suitable for saturable absorber. [5][11] This particular absorber material combined with Nd: YAG gain material was demonstrated by Raikkonen et. al. in 2008 [11] producing 4 ns pulses with 12 kHz pulse repetition rate and 5 µJ pulse energy allowing good combination of pulse energy and pulse repetition rate in over ten Kilohetrz range from the seed laser itself.

For 1.3 - 1.5 µm wavelength region Co:$MgAl_2O_4$ (Co:MALO) absorbers have been widely demonstrated. Very short pulse durations and high energies, such as 1 ns [12] and 2.7 - 10 mJ [13] have been demonstrated using Co:MALO absorbers. These absorber materials have excellent damage threshold and thus can be used to produce high energetic pulses. Alternative Co^{2+} based absorbers include $e.g.$ Co:YAG, Co:LMA, or Co:ZnSe. These materials are very typically seen in the development of Er- based lasers at 1534 nm. [14] Results with the different Co based absorbers vary from extremely high energies to rather short pulses and high pulse repetition rates. For example, Chinn et. al. [15] recorded peak powers up to nearly 40 kW with kHz pulse repetition rate. Similarly Denker et. al. [16], reported pulse repetition rates up to 70 kHz with Er-based materials and Co -absorbers.

Different solid-state absorbers have been widely in use, both in academic and commercial use for decades. Nowadays the most used ones include the Co -based absorbers for the 1.5 µm region and the Cr:YAG for 1 µm region. There are also others, depending on the use case but these were picked for this thesis with the target of covering the most typical

options with an emphasis on the options for the eye-safe 1.5 µm region. Table 2.1 shows the most typical solid-state saturable absorbers for 1.5 µm and 1 µm region with their upper state lifetime and damage threshold.

Table 2.1. *Typical solid-state saturable absorber materials with their operation wavelength, upper-state lifetime and damage threshold. Combined from [14], [17] and [18].*

Parameter	Co:MALO	Co:YAG	Co:ZnSe	Cr^{4+}:YAG
Operation wavelengths (µm)	1.3-1.5	1.3-1.5	1.3-1.5	1.0-1.1
Upper state lifetime (ns)	350	1	2.9 x 10^5	3.5 x 10^6
Damage threshold [J /cm^2]	7.5	2.5	1.8	900

Co:MALO, Co:YAG and Co:ZnSe are all for the 1.5 µm wavelengths, with different substrates for the Co^{2+} doping. The upper state lifetime for these absorbers varies from ns range all the way to ms region, offering different use cases for the absorbers. Damage threshold on the otherhand is rather close to one another with some Joules per square cm and highest on the Co:MALO. Due to this purpose the Co:MALO is often used in high energy lasers targetting low pulse repetition rates. For the 1 µm region, the Cr^{4+}:YAG absorber is as well very often seen in high energy applications. Compared to the Co^{2+} based materials, this absorber has approximately hundred times higher damage threshold. It is thus one of the most used solid-state absorbers in the ns Q-switched high energy lasers.

Overall passive Q-switches are relatively simple components to operate. They do not require complex electronic systems which allows for a compact and robust footprint. They are low cost compared to alternative options but cannot produce as accurate pulsing or generate as high a pulse energies as active Q-switching methods.

2.3 Passively Q-switched laser

Any laser will require gain, pump and feedback to be operational. Laser gain provides material where first spontaneous and later on stimulated emission can take place. Cavity is needed for the emitted photons to circle around and receive feedback and pump energy is required to initiate the cycle and offer energy for the energy level transitions. [8][5] In terms of pulsed lasers, the pulsing element needs to be included within, or sometimes outside the cavity. For passively Q-switched lasers the saturable absorber is inserted inside the laser cavity. For typical Q-switched lasers the cavity is formed between two mirrors, one of which can be curved to better support the lasing. The required elements, such as the gain medium and the saturable absorber can then be included between these two mirrors as shown in picture 2.6 below.

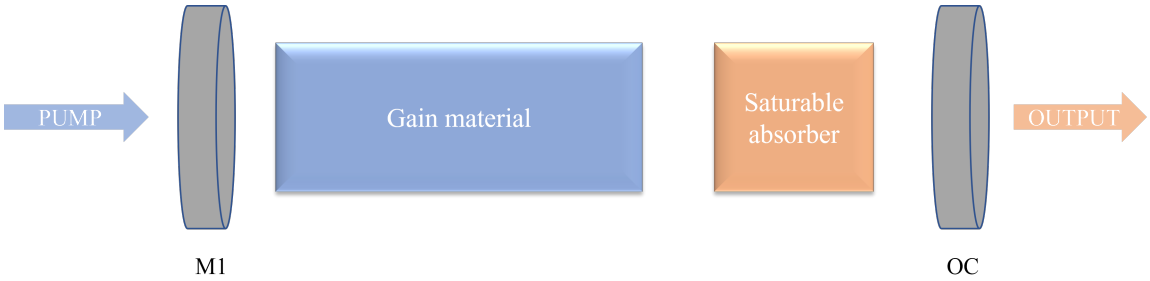

Figure 2.6. *Schematics of a passively Q-switched laser cavity with mirrors M1 and OC.*

In the figure above, mirror 1 (M1) has high reflective (HR) coating for the lasing wavelength and an highly transmission (HT) for the pump wavelength to allow for maximum transmission of pump into the gain. Mirror 2, in the schematics marked as output coupler (OC) is typically a partially reflective (PR) mirror keeping most of the energy within the cavity but allowing for some lasing to exit the system. Typical output couplers vary from 1 % all the way to 20 - 30 %. This value needs to be defined and tested for each laser cavity as it depends on the gain and losses caused by the gain and saturable absorber. The overall losses including the OC need to be in line with formula 2.1 for the lasing to take place.

The benefit of separate components in the cavity structure is that they can be tuned, or changed if needed. One can also add additional components into the cavity, such as intracavity frequency conversion, or etalons for wavelength tuning. [19] The downside of this concept is that each laser cavity must be specifically aligned and the laser may be very delicate to the alignment, meaning it would need to be operated in stable conditions. It also naturally extends the cavity length, lengthening the possible pulse durations available as will be seen later on. Thus a concept for short cavity lengths, using bonded components known as microchip lasers was introduced.

2.4 Microchip lasers

Microchip lasers consist of a a cavity structure, where the cavity is formed around a piece of solid-state gain material. Typically the mirrors are optically coated on the polished end surfaces of the gain. Laser cavity can be a flat-flat or a flat-curved cavity and the system is typically pumped with a semiconductor laser diode. [19] Structure of the most simplistic flat-flat microchip cavity is illustrated below in figure 2.7.

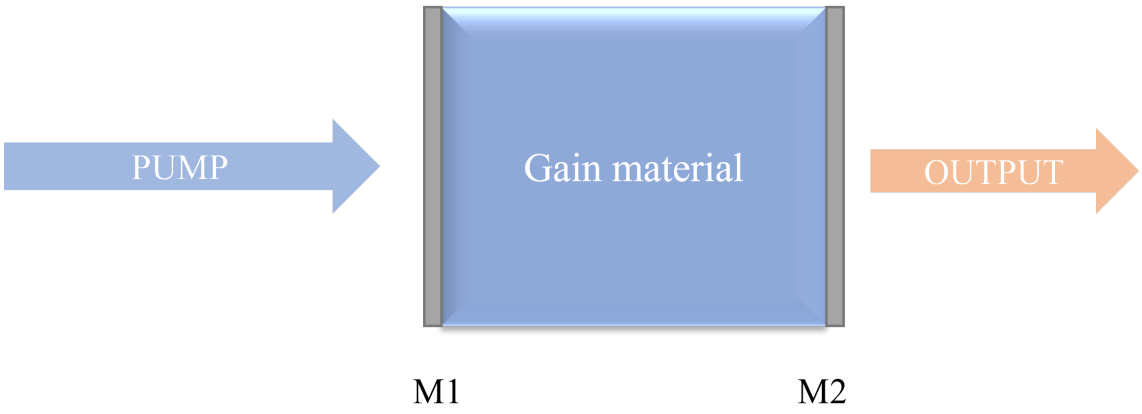

Figure 2.7. *Schematics of a simplistic microchip laser cavity consisting of a gain material and mirrors M1 and M2, which are coated on the optical surfaces of the gain.*

Flat-flat cavities are not especially known for supporting stable operation, which is why typically one of the mirrors is curved. In the case of microchip lasers, thermal lensing effect in the gain material stabilizes the laser cavity, supporting operation with flat-flat surfaces. [19]

For pulsed operation of microchip lasers, additional components need to be included within the cavity. Q-switching of a microchip laser can be performed by adding an active Q-switching element, such as a tunable etalon with partially reflecting mirrors, shown by Zayhowski. [19] A much more straightforward way of pulsing a microchip laser is to use passive Q-switching. Passively Q-switched microchip lasers do not require any switching electronics and can thus be much more compact and cost-effective than alternative options. They can also be structured in a very compact package and allow for mass-production. [19] Passive Q-switching of a microchip laser is performed by adding an intracavity saturable absorber into the system. Schematics of such a laser cavity is shown below.

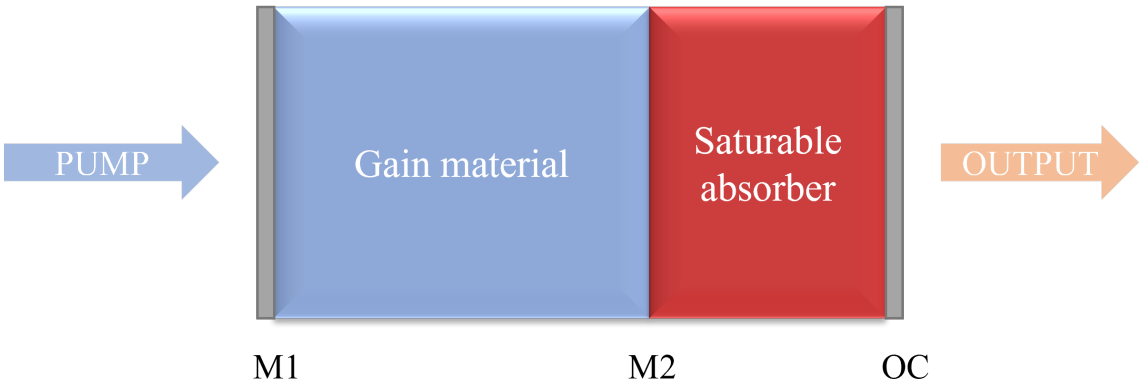

Figure 2.8. *Schematics of a microchip laser cavity with gain material, Q-switch and mirrors M1, M2 and OC.*

The basic structure of Q-switched microchip cavity is very similar to a normal Q-switched laser cavity. The components are compressed between two mirrors, again M1 and OC in

the figure below. M1 is a HR/AR mirror for the laser and pump wavelength, respectively. OC mirror again extracts a small portion of the energy outside the system, seen as the external lasing. Main differences are that all the components are connected to one another, either by bonding or by pressing. Another difference comes from the M2 mirror, not present in typical Q-switched cavity such as 2.6. The purpose of M2 is typically to act as a HR for the pump and AR for the lasing, preventing pump absorption from heating the saturable absorber. [15] The use of microchip cavity allows for a much shorter cavity length, typically from 100 µm to few millimeters. This naturally supports a shorter pulse duration as the cavity length has a linear factor on the laser pulse duration as shown by Zayhowski [19] in equation 2.2:

$$\tau = \frac{8.1\tau_{rt}}{ln(G_{rt})}, \tag{2.2}$$

in which τ_{rt} is the round-trip time around the cavity and G_{rt} is the gain allowed within the round-trip.[19] With the microchip cavity structure pulse durations down to 16 ps have been shown with Nd -based materials [9] and down to 700-800 ps with Er -doped materials [15][20].

2.5 State of the art

Commercial state of the art solutions for passively Q-switched lasers include many options in wavelengths, pulse repetition rate, pulse energy and pulse duration. Typical products operate on Nd -based materials at 1050 - 1064 nm with repetition rate from few hertz up to some tens of kilohertz. Different wavelength regions can be accessed using alternative gain materials, such as Er-based materials in the 1.5 µm region. Wavelength offering can also be widened using second or third-harmonic nonlinear effects.

Directly from the oscillator, energies up to 1.5 mJ can be offered from AlphaLAS PULSELAS P-series at 1064 nm, producing 800 ps - 1 ns pulses with pulse repetition rate of 10 - 20 kHz. This corresponding peak powers up to 1.5 MW.[21] Even higher energies, exceeding 45 mJ can be accessed by utilizing different stages of power amplifiers. Especially in the industrial applications of welding and cutting as well as in pumping of different lasers, long lifetime and extremely high energies are required. Coherent Revolution has been targeted for this purpose, offering up to 10 kHz pulse repetition rate with 45 mJ energy at 527 nm. [22]

For many applications the pure power is not sufficient but for example pulse repetition rate plays an important role in measurement time. Thus, there is a need for higher pulse repetition rates in the hunderds of kHz region. Teem Photonics SNP-130F-1XO offers pulse repetition rate from few tens of kHz up to 130 kHz. By utilizing microchip technology, these products are capable of offering short pulse duration varies all the way from 130 ps to few ns, and depending on the model pulse energies up to µJ level. [23] Bright Microlasers are offering compact solutions for a variety of applications with wavelengths

from 1064 nm to 213 nm. These lasers can provide pulse durations between 300 ps and few ns with output energy up to 80 µJs. The pulse repetition rate can be increased to 100 kHz with 2 µJ pulse energy. [24]

One of the most compact passively Q-switched lasers on the market is the Horus laser by Leukos. This device operates at 1064 nm or 532 nm with ns pulses and maximum energy up to 18 µJ. Laser is especially interesting due to its lightweight down to 100 g and external trigger capability, which is not given for all passively Q-switched lasers.[25] Table 2.2 combines the optical parameters of the state-of-the-art passively Q-swithed lasers at 1064 nm.

Table 2.2. *Commercial state-of-the-art passively Q-switched lasers at 1064 nm.[21]–[25]*

	Pulse duration (ns)	Repetition rate (kHz)	Pulse energy (µJ)
AlphaLAS PULSELAS P-series	0.8-1	10-20	1500
Coherent Revolution	150-220	1-10	45000
TeemPhotonics SNP-130F-1XO	1.4	130	1.5
Bright Mircolasers	400	100	2
Leukos Horus	1	20-30	12

Typically passive Q-switching for high energy applications and ns -region pulse duration is conducted with solid-state absorbers as discussed before. Such absorbers, as the Co:MALO or Cr^{4+}:YAG offer high damage thresholds but can be limited in pulse repetition rate. The highest repetition rate with Co:MALO absorbers is recorded by Denker et. al. [16] at 70 kHz with 1.4 kW peak power. Typically though the repetition rates are in the range of hundreds of hertz to few kilohertz as reported by Qi [14].

To reach a new range of parameters, alternative absorber materials need to be considered. One of the options widely demonstrated in academia is to use semiconductor saturable absorber mirrors (SESAM) as the Q-switch. In many cases this offers more tunability and different parameter combinations compared to solid-state absorbers.

2.6 SESAM - semiconductor saturable absorber mirror

SESAMs are semiconductor components typically faced with lasers as the pulsing components. SESAMs are mostly used in mode-locking, where a vast number of the femto- and picosecond fiber lasers utilize SESAMs for pulsing. SESAMs can also be used as a passive Q-switch in lasers, as demonstrated multiple times over the years. [26] [10][9]

A SESAM typically consists of a substrate, on top of which there is a semiconductor

mirror structure, called Bragg mirror. On top of the mirror, there is an absorber layer and on the front surface typically optical coatings. [27] [10] Figure 2.9 shows a typical SESAM structure with the average thicknesses of each layer.

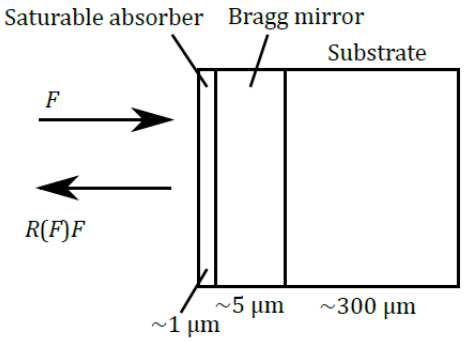

Figure 2.9. *Schematics of a SESAM structure. [10].*

As seen in figure 2.9, substrate is typically the thickest part of a SESAM structure. It is often gallium arsenide (GaAs) for 1 µm region or indium phosphate (InP) for 1.5 µm wavelength region. Basically the substrate is chosen on the operation wavelength aiming for lattice match to generate sustainable absorber structures on top. Next layers include a semiconductor Bragg mirror and saturable absorber, which typically have thicknesses of a few microns. An absorber can consists of quantum wells or bulk material absorbing the photons on the operation wavelength. The top surface of a SESAM can have different optical coatings, for example for pump blocking purpose. [10]

Compared to solid-state absorbers, a notable detail is that in SESAMs, typically the signal is reflected back to the original direction, rather than directed through the substrate. This changes the laser cavity structure of SESAM based lasers compared to solid-state absorbers. This feature will be further discussed later on. Since the signal is typically reflected in SESAMs, also the change of Q-factor is considered as change in reflectance. Figure 2.10 shows a typical nonlinear reflectance of a SESAM.

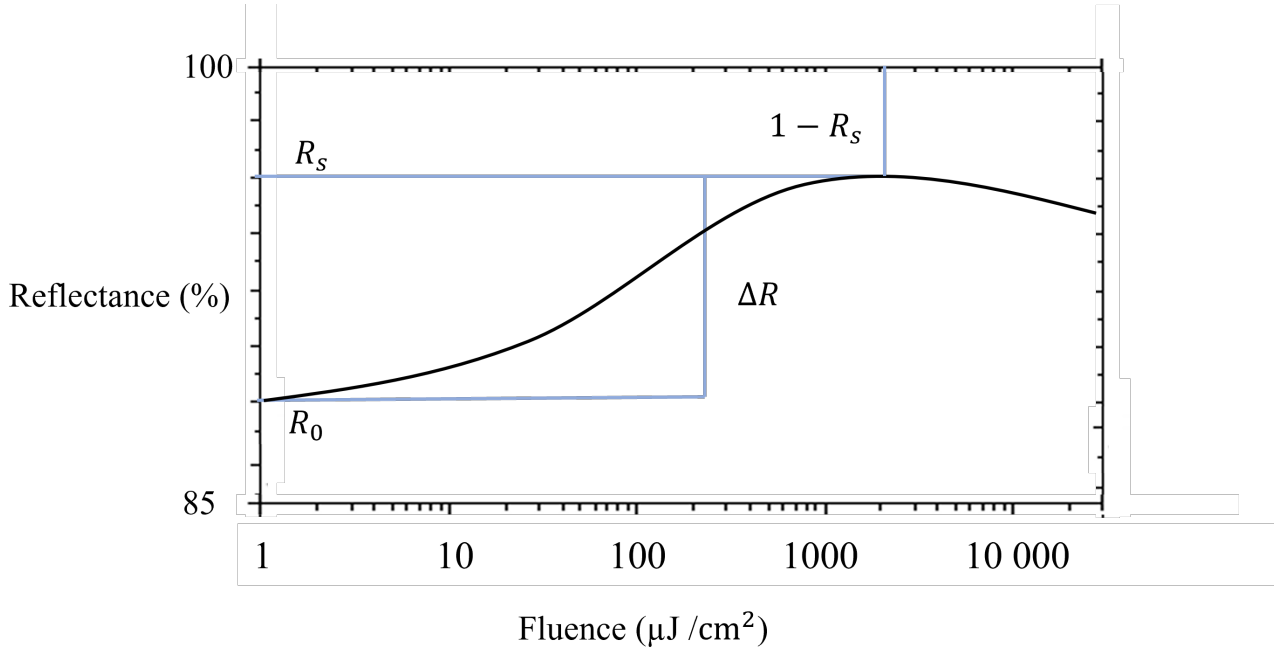

Figure 2.10. *Nonlinear reflectance of a SESAM. R_0 shows the initial reflectance and R_s the saturation reflectance. ΔR is the difference between these two points, called modulation depth.*

Figure 2.10 illustrates a typical nonlinear reflectance of a SESAM. Reflectance is shown as a function of fluence J/cm^2. Reflectance starts at level R_0, namely around 88 %. As the SESAM faces photon fluence, it rises up to the saturation value R_s in the 96 % region. The difference ΔR between R_s and R_0 is called modulation depth and describes the total modulation capability of the semiconductor. As noted before, the saturation value reaches reflectance of approximately 90 %. The remaining reflectance, i.e. 1-R_s are nonsaturable losses in the semiconductor. These are typically unwanted, as they are additional losses in the cavity and cause heat. [10][5]

When compared to solid-state absorbers, the clear benefits allowed by SESAMs is the short length of the absorber. As shown in formula 2.2 the cavity length in Q-switched lasers has a linear factor on the pulse duration. Since the SESAMs optical structure is in the range of few hundred microns, it can support pulses down to sub-100 ps region when combined with a microchip structure, compared to solid-state absorbers typically in the mm range. [10] The semiconductor structures can be fabricated in large amounts which makes them attractive for mass production across a widespread field of applications.

2.7 SESAM Q-switched microchip lasers

In comparison to traditional microchip lasers, also SESAM microchip lasers typically consist of two flat-flat mirrors. One of the mirrors is inserted on top of the gain material and the SESAM structure acts as the second end of the cavity. [28] Additional mirrors can be added within the laser cavity, e.g. to prevent excess heating of the semiconductor. Figure 2.11 shows the schematics of a SESAM microchip laser cavity.

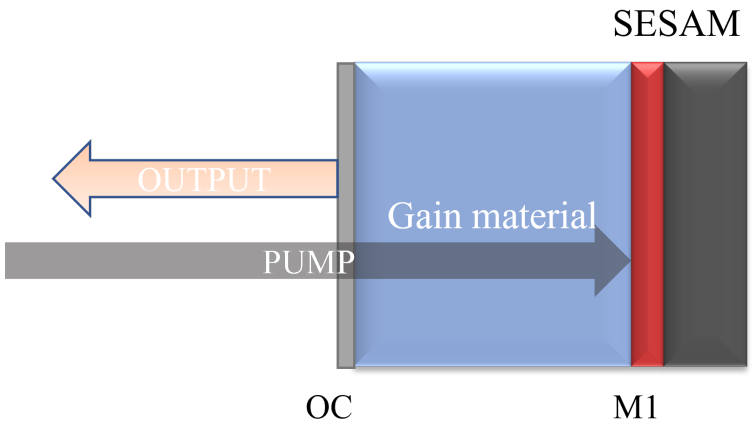

Figure 2.11. *SESAM based microchip laser cavity structure*

The benefits of using SESAMs as the saturable absorber, instead of solid-state absorbers is to allow for higher tunability of the absorber, as well as use of shorter cavity lengths. For example in nonlinear conversion the pulse duration is a critical parameter as it has a linear factor on the peak power of the pulses, thus effecting the conversion efficiency, as will be seen later on in 3

In the quest of shorter pulses, the options are indeed limited to a couple of laser properties; cavity length and absorber modulation depth. When using solid state absorbers, the length of the absorber is typically in mm range, always extending the pulse duration into ns regimes. SESAM structure can be down to few microns and it has thus allowed demonstrations of the shortest pulses generated with microchip lasers, down to 16 ps at 1064 nm. [9] [10] In the framework of this thesis, the aim was to have good control over the microchip laser, allowing for accurate tuning of different pulse properties, such as pulse duration and repetition rate, aiming to find the optimal combination for nonlinear conversion.

3 NONLINEAR CONVERSION

Nonlinear conversion is a phenomenon, where the optical properties of a material are changed by light interaction. The effects are nonlinear as they have a nonlinear dependency on the intensity of light encountered. Many of the phenomena related to nonlinear effects are often encountered with lasers, as they tend to have sufficient intensity for effects to take place. [29]

In relation with lasers, nonlinear conversion has the benefits of allowing more wavelengths than fundamentally available. Especially when considering typical Q-switched lasers operating with solid-state gain media, such as Nd or Er-based materials, the transitions in the gain are the only fundamental frequencies allowed. This causes some limitations on the wavelengths and thus limits the applications, even though the pulse repetition rate and laser peak power could be viable for the application.

Nonlinear phenomenon offer also other benefits and direct applications besides extending the wavelength offering. For example in nonlinear optical microscopy the nonlinear process is utilized in enhancing imaging resolution. Since the nonlinear process is strongly dependent on the intensity, by focusing the light onto a tight spot, only the very focus point will face the nonlinear effects increasing imaging resolution in both transversal and longitudinal axis. [29] The scope of this thesis is to focus on second and third order nonlinearities to show the usability if these phenomenas in producing application specific laser sources.

3.1 Second-order nonlinearities

Nonlinear effects can be characterized by order of nonlinearity, i.e. by the number of waves interacting with one another. The simplest cases come with the second-order of nonlinearity, such as sum-frequency generation or second-harmonic generation, in which two waves interact with each other, forming a third wave. [5] The general form of sum frequency generation can be illustrated as shown in figure 3.1.

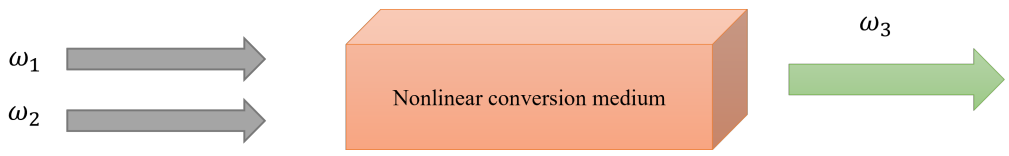

Figure 3.1. *Sum-freqency generation.*

As the sum of frequencies must be equal on input and output, the sum frequency generated can be written as [5]:

$$\omega^1 + \omega^2 = \omega^3 \tag{3.1}$$

As a special case of the three-wave interaction, there is second harmonic generation (SHG), where the incoming waves ω^1 and ω^2 are the same, namely ω. [29] In this case the sum frequencies can be described as:

$$\omega + \omega = 2\omega \tag{3.2}$$

Light interaction of the two photons in the form of energy diagram has been shown by Nikkinen in 2017. The two absorbed photons are emitted as one with frequency double to the original as shown in 3.1.

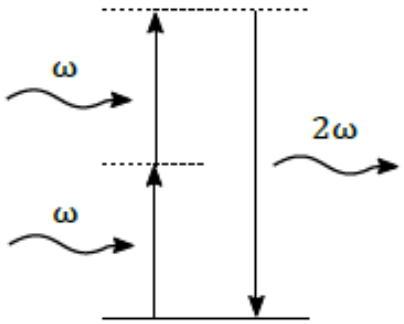

Figure 3.2. *Second harmonic generation energy diagram. Modified from [10].*

In practise, the principle of second harmonic generation leads to the fact that there can always be less photons emitted as 2ω than in ω. Typically the conversion efficiencies seen in SHG can rise up to 80 %. [5]

3.2 Third-order nonlinearities

The same principle can be applied also to higher order of nonlinearities, such as third-order effects. In the third-order, three different waves can interact causing the generation of a fourth wave. As the order of nonlinearity increases, the need for higher intensities rises simultaneously.Typical third order optical effects include third harmonic generation and Raman effect. [5][29]

In the third harmonic generation, three identical photons interact with one another generating a fourth one with a frequency equaling the sum of all three. Third harmonic generation can thus be interpreted as [5]:

$$\omega + \omega + \omega = 3\omega \tag{3.3}$$

Third harmonic generation is a very typical way of generating frequencies that are normally hard to achieve. The most commonly known third harmonic generation is generating frequencies in the UV from 1 µm. E.g. 354.6 nm wavelength in the UV region can be accessed by third harmonic generation of 1064 nm lasers, which are widely available.

Another example of a third order nonlinear phenomena is stimulated raman scattering (SRS). In SRS the interactions of light and molecular vibrations either redure or increase the energy of the photons and thus change their frequency. Stimulated Raman scattering can be thus divided into two parts. In the first one, the incoming photons give energy to the vibrating molecules and the emitted photon thus has a smaller frequency. This process is called Raman Stokes scattering. The countering version for Stokes is called anti-Stokes, in which the vibrational energy of the molecules is added to the photon and the frequency thus increases. [10] Both Stokes and anti-Stokes scattering are described in figure 3.3 below.

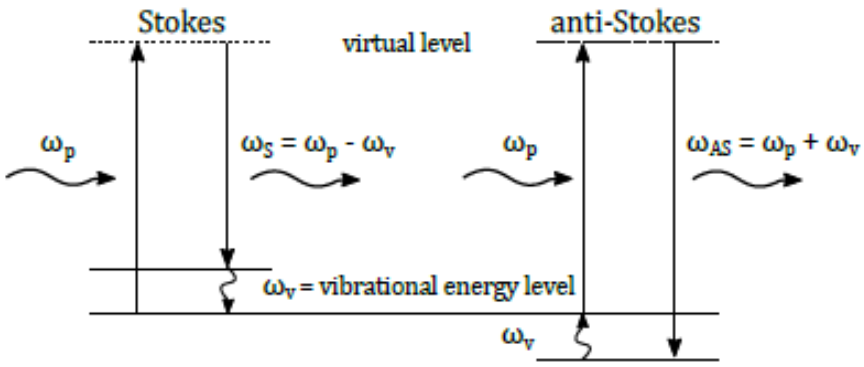

Figure 3.3. *Energy diagram of the two parts of stimulated Raman scattering, Stokes scattering and anti-Stokes [10].*

All of the phenomena discussed above, take use of light-matter interaction. They require a high number of photons for the frequency conversion to take place, because the probability of the nonlinearity taking place is not high. However, there are additional requirements to the material, in which the nonlinear phenomena can take place, such as phase matching and damage threshold. Materials should also allow for easy usability and thus come typically in the form of solid-state structure. These properties and requirements will be discussed in the following.

3.3 Phase matching

In order to achieve high frequency conversion efficiency, the fundamental and the generated harmonic frequencies should be able to travel nearly coherently distances far greater than the typical coherence length of typical crystals. The interaction length of these waves

increase the harmonic power output by a factor of square, making it a very crucial parameter for decent conversion efficiencies. For this requirement to be fulfilled, the two waves should have a refractive indices as close to one another as possible in the conversion material. [5] This means that the sum of wavenumbers would equal to zero, i.e. $\Delta k = 0$. This can be also referred as the phase-matching condition [10]:

$$n_1\omega_1 + n_2\omega_2 = n_3\omega_3. \tag{3.4}$$

Typical way to fulfill the phase-matching condition is to use uniaxial crystals as the nonlinear material. These birefringent crystals can have same refractive indices for different wavelengths on different crystalline axes. [10] [5] This allows the two waves to travel coherently throughout the crystal producing effective frequency conversion.

Phase matching can be divided into to categories, type I and type II. In type I the polarization of the two waves is the same, as in type II it is orthogonal to one another. In this thesis we will look only into type I phase-matched crystals due to their general popularity. Typical phase matching parameters for a nonlinear crystal are the acceptance angle, in which the phase matching can be achieved and operation temperature, which can be used to tune the phase difference. [5]

Besides phase matching, the requirement of having the two waves travel coherently can also be allowed with different crystalline structure. Quasi-phase matching (QPM) is a method to fulfill the conditions for phase matching by changing the sign of nonlinearity in the crystal after a certain period. In QPM, the propagating waves are allowed to face some phase mismatch for a certain period, but the nonlinearity is reversed before the conversion would fall back into the fundamental wave. [10][30] The basic principle of changing the sign of nonlinearity is illustrated below in a picture by Dr. Paschotta:

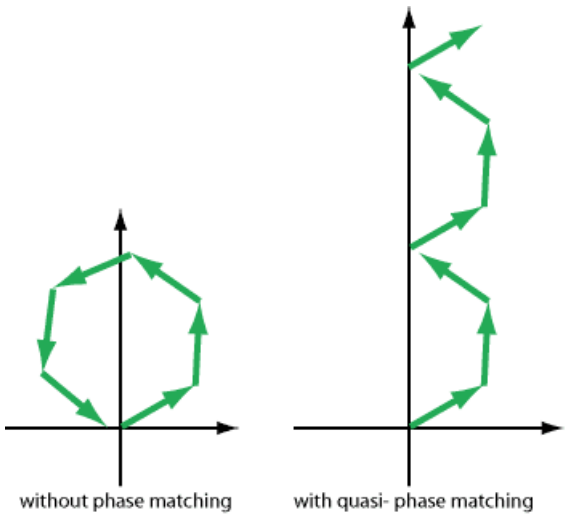

Figure 3.4. *Change of nonlinearity in quasi-phase matching. Modified from [30].*

QPM is typically produced by making a periodically poled crystal for frequency conversion. The biggest benefits of QPM based frequency control is that it allows for a use of materials where the normal phase matching conditions would not be satisfied, widening the spectrum of materials and thus also frequencies that can be used. For nonlinear crystals the main properties of interest are related to their ability to fullfill the phase matching conditions, as well as their mechanical and thermomechanical properties.

3.4 Nonlinear crystals

Besides the ability to allow phase matching, nonlinear crystals are required to have wide optical transparency and acceptance angle, high damage threshold, large nonlinear coefficient and good homogeneity. [10] By these standards, some of the most popular second harmonic conversion crystals based on birefringence are monopotassium phosphate (KDP), beta barium borate (BBO) and lithium triborate (LBO). Most popular nonlinear crystal based on the quasi-phase matching is periodically poled lithium niobate (PPLN). This thesis will cover the main properties of these crystals, keeping the emphasis on the PPLN, as this was the crystal used within the experimental work in this thesis.

3.4.1 KDP

One of the most popular crystal for frequency conversion is potassium dihydrogen phosphate, KDP. This crystal has an extremely high damage threshold up to 8 GW/cm^2, which is nearly four times more than typical competing crystals. KDP also has very wide transparency between 200 nm and 1600 nm and the birefringence is not too strongly dependend on wavelengths, allowing doubling of broad sources at a wide emission range. [5]

However compared to BBO and LBO, KDP has a low nonlninear coefficient, down to 0.37 ps/V. It is also very sensitive to thermal shocks and needs to be operated at a high temperature due to its water-soluble structure. [5] This often leads to the laser system having batteries or similar connected to the system, preventing any rapid drop of crystal temperature in the occasion of a power cut.

3.4.2 BBO and LBO

Beta-Barium Borate, BBO is one of the nonlinear crystals from the borates. It has nice nonlinear coefficient, good transparency and very high damage threshold. BBO has been demonstrated with conversion efficiency up to 60 $\%$ and due to the good transparency and nonlinear coefficient, it can be typically seen with converting 1064 nm light to visible and all the way to the UV region. [5] Downside of BBO is that it has very low angular tolerance of 0.8 mrad $\times$cm, requiring good beam quality for efficient frequency conversion.

Lithium triborate, LBO is the second typically used borate based nonlinear crystal. It has as well good mechanical structure and transparency. LBOs have higher damage

threshold than BBO, up to 2.5 GW/cm^2. They also can be phase matched with high temperatures, giving large acceptance angle up to 8.5 mrad$\times$cm, which is about ten times higher than with BBO. [5]

3.4.3 $LiNBO_3$ and PPLN

Fouth type of material, which is of special interest in regard to this work is lithium niobate $LiNBO_3$. Lithium niobate has high nonlinear coefficient, up to 4.7 pv/V, but requires high temperatures and is especially vulnerable to photorefractive damage. [5] Nowadays it is not that popularly used as such, but a periodically poled version has gained interest. The most typical properties of these four nonlinear crystals are shown below in table 3.1.

Table 3.1. *Typical nonlinear crystals and key parameters. Modified from [5]*

Parameter	KDP	BBO	LBO	$LiNbO_3$
Nonlinear coefficient [pm / V]	0.37	1.94	1.16	4.7
Angle [°]	41,2	22,8	11	90
Angular bandwidth $\Delta\theta$ [mrad$\times$cm]	3.2	0.84	8.5	46.3
Damage threshold [GW /cm^2]	8*	1.5	2.5	0.2

* in the use as second harmonic generation.

The periodically poled version of lithium niobate, PPLN has indeed becomed extremely popular within the recent years. This is mainly due to the extremely good nonlinear coefficient and the use of quasi-phase matching, allowing for much wider region of wavelengths previously unavailable. The main difference in PPLN compared to the previous materials is that the periodic structure of the crystal corrects the phase of the propagating beams every time the nonlinearity changes. The structure of a PPLN crystal is shown below in figure 3.5.

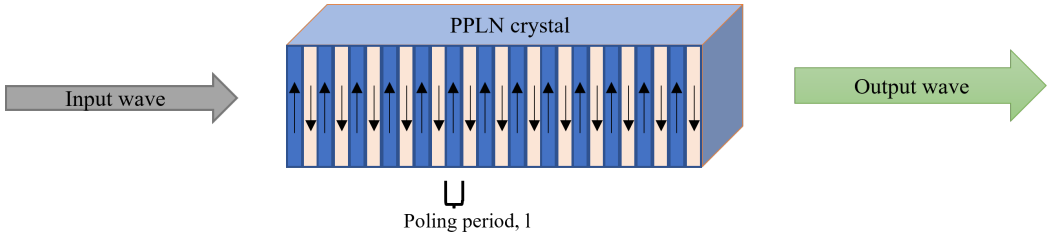

Figure 3.5. *Periodic poling in a PPLN crystal. The arrows point out the direction of nonlinearity. Distance l marks the poling period.*

The distance l of different nonlinearity is called poling period and corresponds to the distance shown in figure 3.4 in which the phase-matching is corrected. This affects the nonlinear generation in steps as the light passes in the medium. This effect in QPM PPLN is illustrated below:

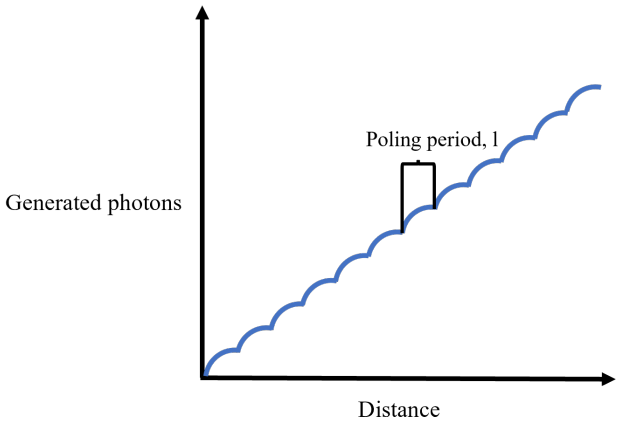

Figure 3.6. *Quasi-phase matching photon generation in PPLN nonlinear conversion. Modified from [31]*

So in practice the nonlinear photon generation in QPM goes in cycles, where at the middle of each nonlinear sign cycle, the effectiveness of nonliear conversion is at its highest. Then once the cycle goes towards the zero point, conversion slows down and starts up again once the direction of nonlinearity is changed again. This cycle goes on throughout the distance of the crystal, constantly gaining up the generated photons, i.e. in the chassis of this work, the second harmonic frequency of the primary waves.

The downside of PPLN is that it has low damage threshold. Typically it offers high conversion efficiencies though, due to the high nonlinear coefficient, but cannot support operation with high powers. For perspective of this work, PPLN was the ultimate choice as it offered good conversion efficiency with low output power and was able to convert primary wavelengths from the 1.5 µm region into the early NIR I region.

4 EXPERIMENTAL WORK

Microchip lasers have been studied since 1988 when Zayhowski introduced the concept of a flat-flat bonded cavity [32]. Since then, the work has spun around 1 µm lasers to provide a viable option for mode-locked lasers with short pulses but complex structure and 1.5 µm lasers to generate eye-safe lasing for sensing or distance measurements. [28] This generated extremely short pulses down to sub-100 ps region with Nd:YVO_4 gain and GaAs SESAMs as Q-switched [10] and over 10 kW of peak power at the 1.5 µm regime for range-finding applications [28].

A different set of parameters were introduced in 2020 when a SESAM Q-switched Er, Yb-glass based microchip lasers were studied [20] for LIDAR purposes to allow for a tunable, high repetition rate operation in the eye-safe regime. This work introduced kW peak power with repetitino rate upto 50 kHz aiming for UAV LIDAR applications. A further work aimed to extend the measurement resolution, producing pulse repetition rate up to 700 kHz but with a peak power of only 6 Watts. [26]

The experimental work of this thesis aimed to investigate a suitable combination of pulsed laser parameters for microscopy and sensing applications by tuning the SESAM microchip component to generate high peak powers with ns pulse duration and tens of kHz pulse repetition rate. This laser was then frequency converted to the NIR I regime by second-harmonic generation to allow these pulsed properties in action for the challenging 700 - 800 nm wavelength region.

The experimental work focused on developing a tunable, SESAM Q-switched seed laser operating at 1534 nm and to frequency convert this laser to 767 nm. The set of parameters from pulsing perspective were investigated as one part and the conversion efficiency with these parameters as the other one.

4.1 Experimental setup –check!

The experimental setup constructed of a microchip seed laser with optical pumping and focusing optics, as well as collimation and focusing optics for the second harmonic generation after the seed. For optical pumping a single mode, fiber coupled 976 nm laser diode from II-VI was used with output power up to 1 W. This laser was wavelength locked and temperature stabilized, which allowed for accurate analysis of the microchip seed lasers, taking out any variations from the pump. The pump diode optics included a Thorlabs fiber collimator (FC/PC 980 nm Collimation Package) and a changeable focusing lens for quick tunability of the setup. Schematics of the seed laser are shown in figure 4.1

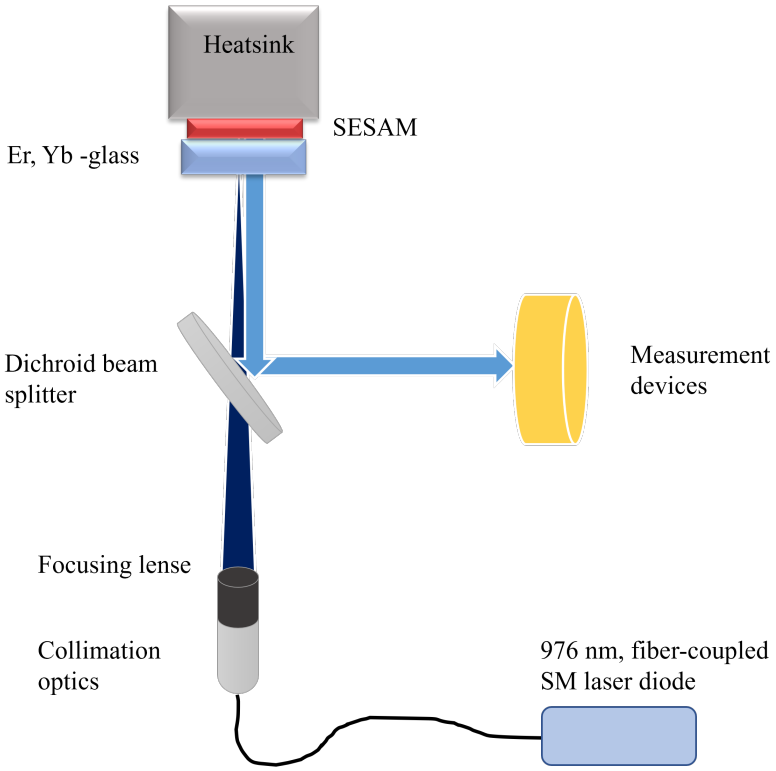

Figure 4.1. *Seed laser schematics.*

Pumping was performed through a 45 degree dichroid beam splitter with low reflectivity at 0 degrees for 976 nm and high reflectivity at 45 degree for the emitted 1534 nm region to split the pump and lasing signals from one another. The microchip seed was mounted on an aluminium heatsink and connected to a Thorlabs 3-axis MicroBlock (MBT616D/M), which enabled tuning of all three dimensions of x-y-z with µm resolution. The pump optics, the dicroid beam splitter and the microchip seed were all mounded on 1" or 0.5" mirror mounts to allow for accurate angle-tuning of the components, individually from one-another. The seed laser lab structure is shown in figure 4.2 below.

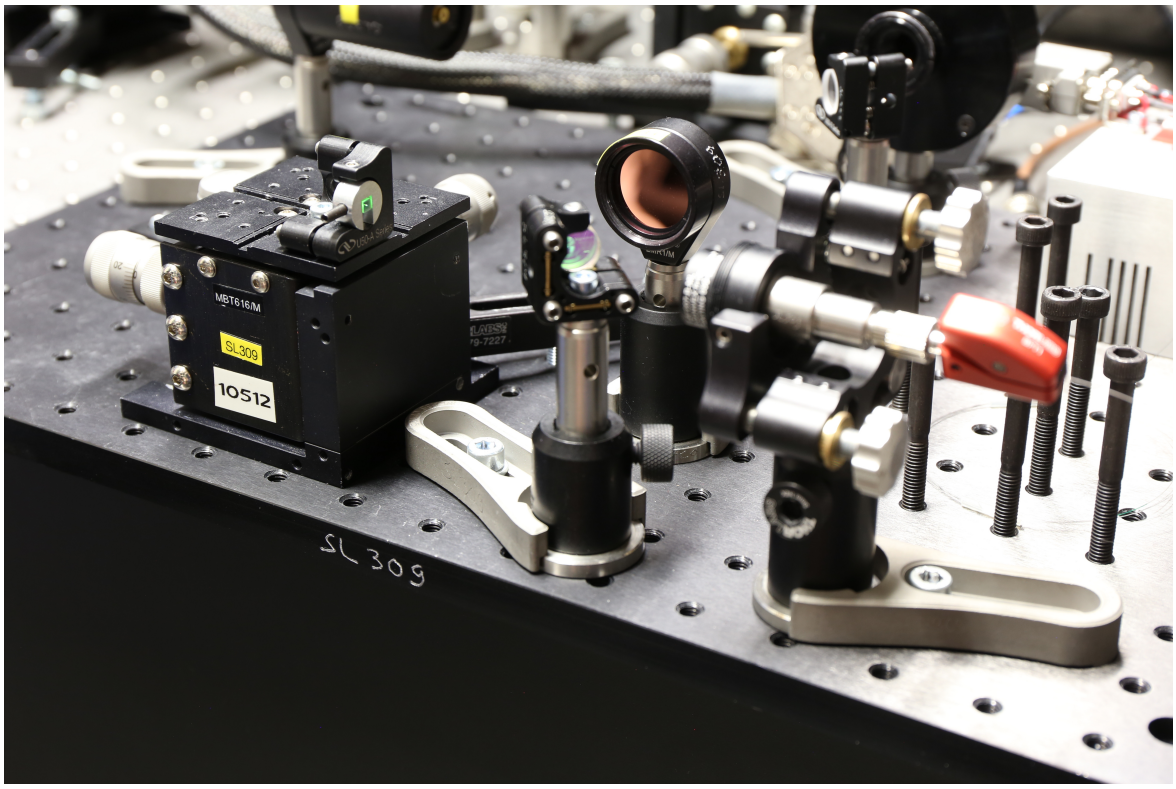

Figure 4.2. *Seed laser pump setup.*

The seed laser was constructed as one piece of the experimental setup and once suitable output from the seed was achieved, further pieces were added to allow for wavelength conversion. For the purpose of second harmonic generation, additional filtering and optics were added to the setup. First the emitted seed laser signal was collimated and further on focused to the second harmonic crystal. With such a setting the focusing size could to the SHG crystal could be altered while maintaining the seed laser setting without any changes.

The second harmonic crystal was a Covesion PPLN crystal with a length of 20 mm and 9 channels for the 1.5 µm operation region. The crystal was mounted on a Covesion temperature stabilized crystal mount and attached to a micrometer stage, allowing for accurate temperature tuning of the crystal while being able to move the crystal with accurate resolution to reach the right channels. Schematics of the complete experimental setup is shown below in picture 4.3.

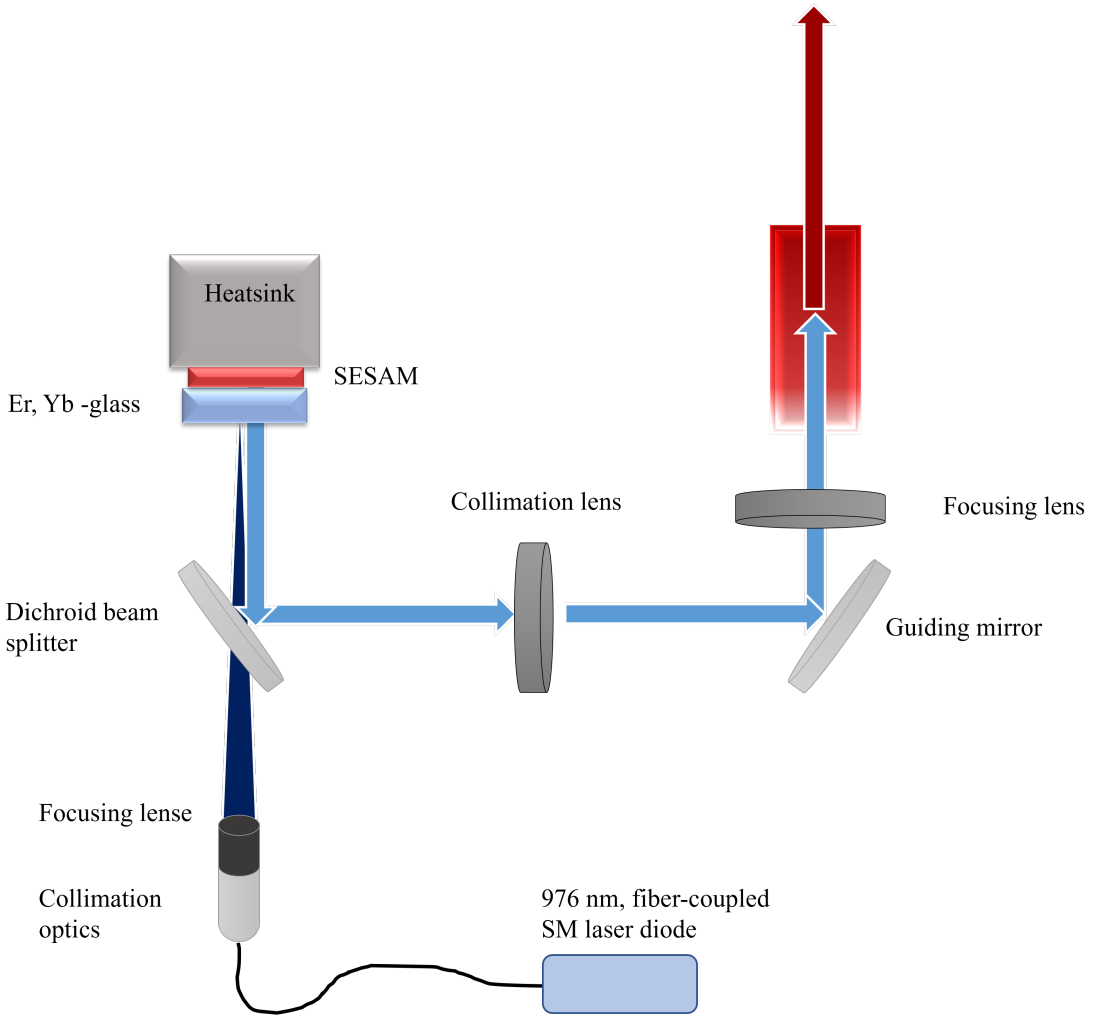

Figure 4.3. *Schematics of the experimental setup.*

The pump laser diode was operated using a Thorlabs Combined Laser diode and TEC controller (ITC4020). The ITC4020 benchtop controller allowed operation up to 20A, 11 V with both, CW and Quasi-CW pumping options. For optical measurements, a Thorlabs 5 GHz InGaAs photodiode (DET08CL/M) with a risetime of 70 ps and a Keysight 1 GHz oscilloscope with 5 GSa/s and a risetime of 550 ps were utilized. Powermeter for 1534 nm in use was a 3W thermal Ophir Optronics (3A-SH) powerhead with the stand-off reading mount. 767 nm power levels were measured with a Si-based PD300 power meter from Ophir Optronics. For spectrum measurements an Ando AQ6317B optical spectrum analyzator was used with a resolution up to 20 pm and spectrum coverage from 600 nm up to 1700 nm.

Within the measurements, several different seed laser combinations, including different pairs of gains and SESAMs were studied at repetition rates of 1 - 5 kHz as well as above 100 kHz. The second harmonic conversion studies on efficiency at different beam sizes and optical parameters were studied along the seed lasers to define the optimum combination in terms of both, seed parameters and conversion efficiency.

4.2 Seed lasers

The seed laser constructed of a Er, Yb -glass based gain material, with varying thicknesses from 0.5 to 1 mm. The glass gain was chosen on the good performance shown by earlier work in [20] [14] generating several kW of peak power and withholding tens of kilohertz pulse repetition rate. Gain dimensions were 3x3 mm to allow for easy handling of the chips. These gain chips were optically clamped or bonded to a semiconductor saturable absorbers, which acted as the Q-switch in these lasers. Below is a picture of the bonded microchip seeds with the gain and SESAM attached to an aluminium heatsink.

(a) *Microchip seed laser chip.* ***(b)*** *Seed laser in operation.*

Figure 4.4. *1.5µm seed laser chips.*

The SESAM Q-switch were constructed on InP substrates using InGaAs absorbing structures. Several different options of Q-switches were studied with varying absorbtion and structure. Optical cavity was structured between the front-surface of the gain glass and the back-structure of the SESAM. Cavity reflectances were manufactured and tuned by ion beam sputtering coater by CEC [33], allowing for a very accurate reflectances at different wavelengths. Optical coatings were typically TiO2 / SiO2, dielectric coatings with output coupler reflectances varying between 80 - 99 %. A typical reflectance spectrum of a seed laser gain is shown below in picture 4.5.

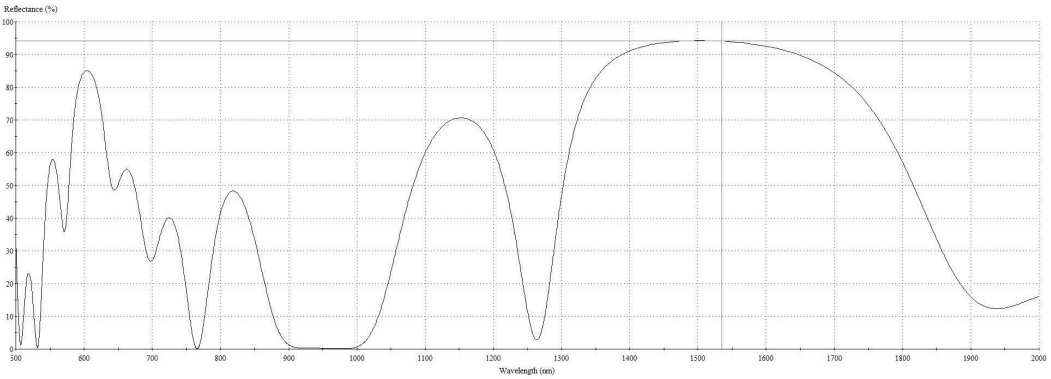

Figure 4.5. *Example of a typical reflectance spectrum of a cavity end coating.*

Coating has an AR structure for the pump region at 980 nm area, and a PR coating for the output coupler between 1500-1600 nm. The coating was typically structured as 2 - 5 pairs of high and low refractive indice materials, in this case TiO2 and SiO2 with refractive index of 2.45 and 1.44, respectively at 1.5 µm wavelength. [34] With this combination and a Essential MacLeod design tool, different optical coatings for filters and output couplers were designed for the laser structure. These optical coatings included the mirrors at the end of the microchip cavity as shown in figure 2.8.

Development of the seed lasers at 1534 nm, included several trials of different SESAM gain combination, with variable optical coatings. Testing focused on short pulsed lasers, with gain medium distance of 0.5 - 1.5 mm, aiming to have high enough peak power for efficient nonlinear conversion. Different parameters of the cavity were tuned to discover the laser limits in terms of pulse parameters. The extended laser parameters of different combinations, in terms of pulse repetition rate, peak power, and pulse duration are presented below in table 4.1.

Table 4.1. *Combination of seed laser parameters during development at 1534 nm.*

Repetition rate (kHz)	Pulse duration (ns)	Peak power (kW)
5	1.1	2.85
10	1.2	2.22
40	1.25	1.26
100	2.58	0.25
315	0.87	0.05
820	0.94	0.03

As showed in table 4.1 above, the variance of parameters possible with the SESAM microchip seed lasers is quite vast. Pulse repetition rate extends from few kHz all the way to nearly over 800 kHz. Pulse duration varies in the range of 1-3 ns and pulse peak power reduces with the increasing repetition rate. In general, the work conducted aimed at keeping the pulse duration as short as possible to generate high peak powers for the nonlinear conversion. However, as the pulse duration is dependent on the cavity length,

some differences can be seen between the seed lasers. For example, the 100 kHz laser utilized a longer cavity, aiming for higher average powers, thus generating much longer pulse duration of over 2.5 ns. Typical pulse duration is shown below in figure 4.6.

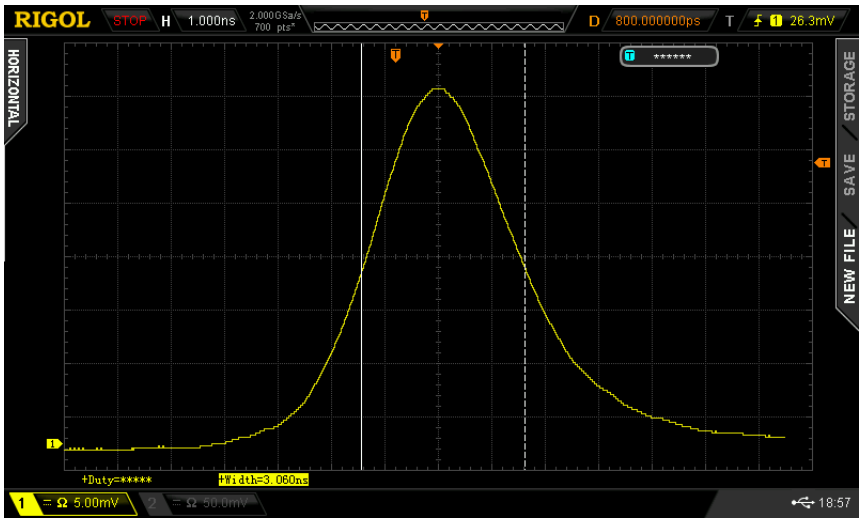

Figure 4.6. *Typical pulse duration of a 1534 nm microchip seed laser.*

Reduction of pulse peak power with increasing repetition rate is very typical, caused by the increasing probability of damage to the laser with more pulses. Pulse peak power varies between 2.85 kW and 30 Watts within this range. For the second harmonic generation, a laser source with higher peak power would be more suitable, and thus the further development focused on pulse repetition rates below 40 kHz.

4.3 Second harmonic generation

To reach a novel wavelength region, considering Q-switched solid state lasers, studies on second harmonic generation of the seed lasers were conducted. These experiments were especially interesting when combined with the pulse parameters generated with the SESAM microchip seed lasers. The aim of the SHG studies was to allow for high as possible conversion efficiency into 767 nm while obtaining the pulse parameters of ns pulse duration and several tens of kHz pulse repetition rate which could be of interest in photoacoustic or LIDAR applications.

For the purpose of second harmonic generation, several conversion crystals were considered. After an evaluation of different options and the operation wavelength of the seed, periodically poled lithium niobate crystals were chosen as the conversion crystals. The advantage of PPLN is that they allow use of long length due to their poling structure, thus typically being able to offer higher conversion efficiencies than the phase-matched options. PPLN normally has a lower damage threshold and requires higher operation temperatures, but in the case of this work, the average powers used were in the range of tens to hundred milliwatts, which is well in the limits of PPLN damage threshold.

The conversion crystals chosen for the tests were Covesion MgO doped PPLN crystals.

Crystal length was decided to 10 mm, aiming to allow for sufficient conversion efficiency and not being too long for the beam to divert. PPLN crystal had 0.5 mm channels with 9 poling periods allowing operation from 1530 - 1600 nm. This crystal was chosen as the main component, as it offered adjustability in case other operation wavelengths were to be studied. Since the PPLN crystals are not phase matched, they are typically operated in higher temperatures than room temperature to allow for accurate phase matching. This causes collateral issues, as the crystal should be heated and mounted at the same time. For easy fix to this issue a crystal mount, oven and temperature controller, designed for the specific crystals by Covesion were all utilized. Especially the crystal mount with a spring-like attachment proved to be essential, since mounting of the long, delicate crystal without it would have required significant work to be conducted. This mount also allows for fixing during heating into high temperatures, which was essential for the measurement, as shown later on. Figure 4.7 shows the crystal and the crystal mount used in the experiments.

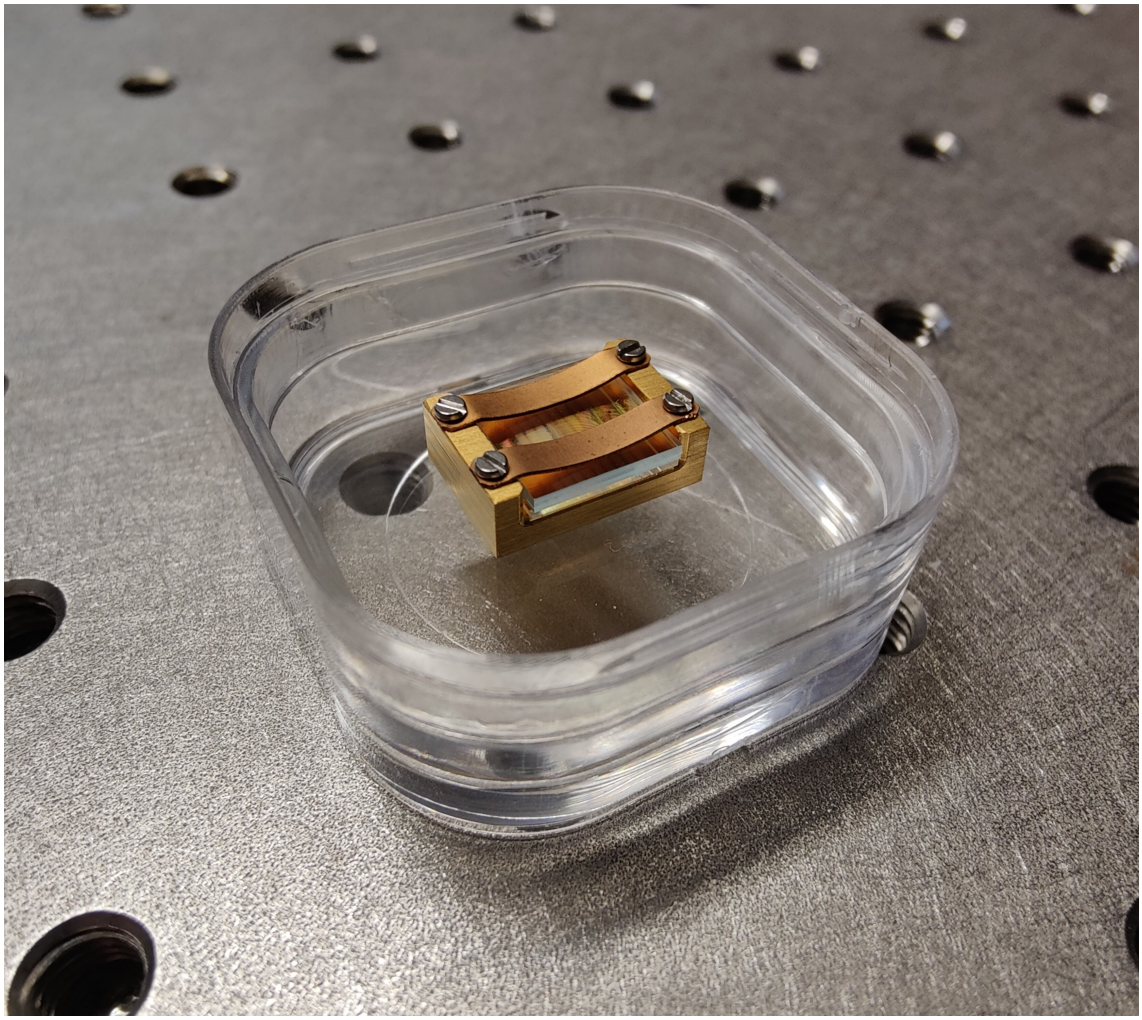

Figure 4.7. *Covesion PPLN crystal and the crystal mount.*

Phase-matching of the quasi-phase matched PPLN crystals is typically conducted by controlling the operation temperature. This allows for use of different wavelengths in the same crystal and even channel, but also requires operation in reasonably high temper-

atures, typically 50 - 100 °C and accurate temperature control. In the crystal used with this thesis, the channel used was with 18.80 µm poling period. This was chosen to operate at reasonable temperatures, which in the tests conducted between 65 - 75 °C. The phase-matching curve of the MSHG1550-0.5 crystals is shown below in figure 4.8.

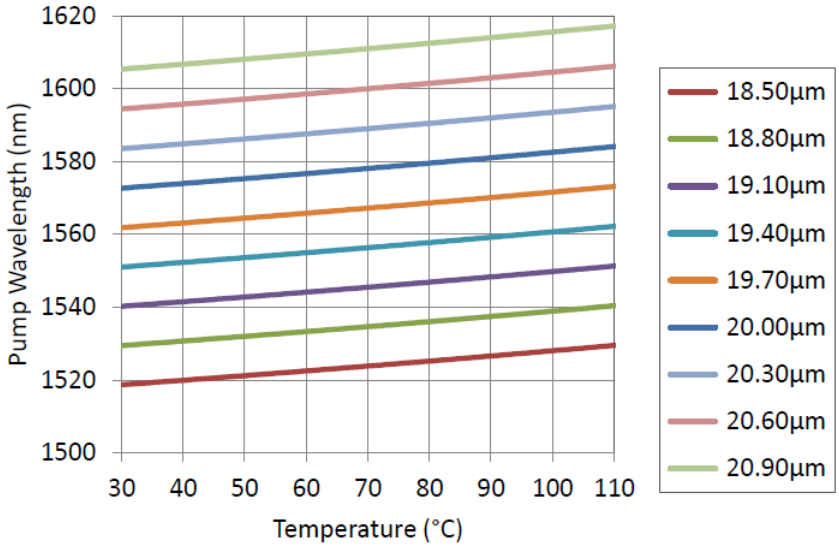

Figure 4.8. *Phase matching curve for the PPLN crystal. [35]*

In the work of this thesis, the second channel of the PPLN crystal was used. This equals to a poling period of 18.80 µm and is shown as the second from below in the figure. This channel was chosen as it allowed operation at the 1534 nm wavelength at temperatures of approximately 75 °C. Since the crystal is optimally targeted for operation at 1550 nm wavelength, no other channels offered good wavelength fit for the 1534 nm.

For the optimal conversion efficiency, to provide usable power levels after the second harmonic at 767 nm only primary lasing at repetition rates up to 40 kHz were considered. Higher pulse repetition rates were studied, but they rapidly showed much lower frequency conversion efficiency and thus were neglected from SHG studies. For the seed laser, the targeted peak power was over 1 kW.

A broad coverage of pulse repetition rates between 5 kHz and 40 kHz were chosen for the SHG studies. All lasers were targeted to have short pulse duration below 2 ns, for the peak power to stay in decent numbers. Different focusing lenses for the second harmonic were studied in order to achieve the highest conversion efficiency. The best conversion efficiency was found with beam waist of 46 µm at the center of the nonlinear crystal. Different beam waists were studied between 30 and 65 µm but the 46 µm proved to provide the best efficiency. Table 4.2 shows the pulse repetition rate, peak power and pulse duration of frequency converted 767 nm with this particular beam size.

Table 4.2. *Frequency converted output to 767 nm.*

Repetition rate (kHz)	Pulse duration (ns)	Peak power (kW)	Conversion efficiency (%)
5	1.1	1.8	57.3
10	1.2	1.4	52.4
40	1.25	0.83	57.8
100	2.18	0.09	31.4

Conversion efficiency up to 57.8 % was achieved, when a primary lasing power of 63.1 mW was converted to 36.4 mW with 40 kHz pulse repetition rate. Typically the conversion efficiency varied between 52 - 58 % which can be considered a reasonably good result for a seed laser conversion with ns pulses. It should be noted that it is exceptional that the 40 kHz pulses results same conversion efficiency as the 10 kHz, but this may be due to thermal effects in the crystal or by the great number of average power seen. In comparison, the dependency of conversion efficiency on peak power is seen with the 100 kHz laser, where the efficiency is greatly lower due to longer pulse duration and higher pulse repetition rate.

Intensity variation is a very typical downside of passively Q-switched lasers, as the pulses are formed independently. The effect tends to reinforce as the nonlinear conversion is taken into use, as every difference with the primary waves goes through nonlinear process, highly dependent on the intensity. Thus the more powerful pulses gain better conversion as the weaker ones, increasing the difference between these. Figure 4.9 illustrates the typical intensity variation faced with the 767 nm lasers in this thesis.

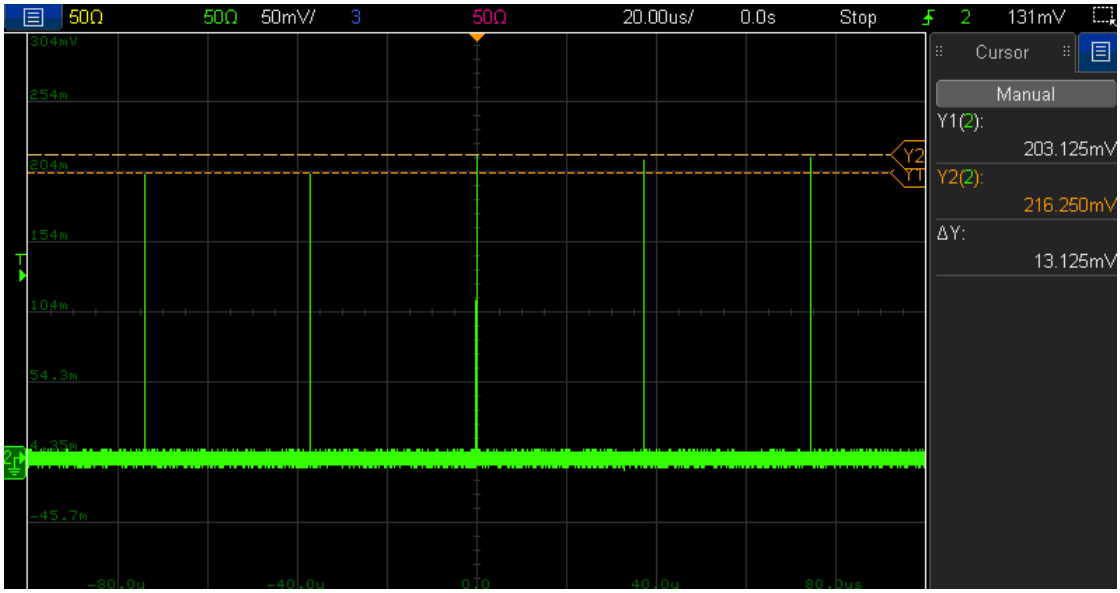

Figure 4.9. *Typical pulse to pulse intensity variation of the 767 nm pulses.*

Figure 4.9 shows a typical intensity variation of a frequency doubled microchip laser at 26 kHz pulse repetition rate. With the difference of 13.125 mV between the highest, 216.25 mV and the lowest pulses, 203.125 mV as seen the figure, the percentual variation is

approximately +/- 3.1 %. This is a very normal value for a passively Q-switched laser, taking into consideration the fact that the nonlinear effect increases the normal differences between pulses.

Another typical disadvantage of passive Q-switching is the timing jitter between pulses. Timing jitter is not dependent on the second-harmonics, as the intensity variation, but relates to the pulse repetition rate of the lasers. As the studied lasers are optically pumped with quasi-cw pumping, the duration of pump energy needed, depends on the pulse repetition rate. Thus, with smaller pulse repetition rates, as needed for the higher pulse peak powers, the pumping time is extended. This often leads to larger timing jitter, between pulses, as the laser pulses have a larger time window to be emitted in. Typical timing jitter of the generated 767 nm pulses is shown below in figure 4.10.

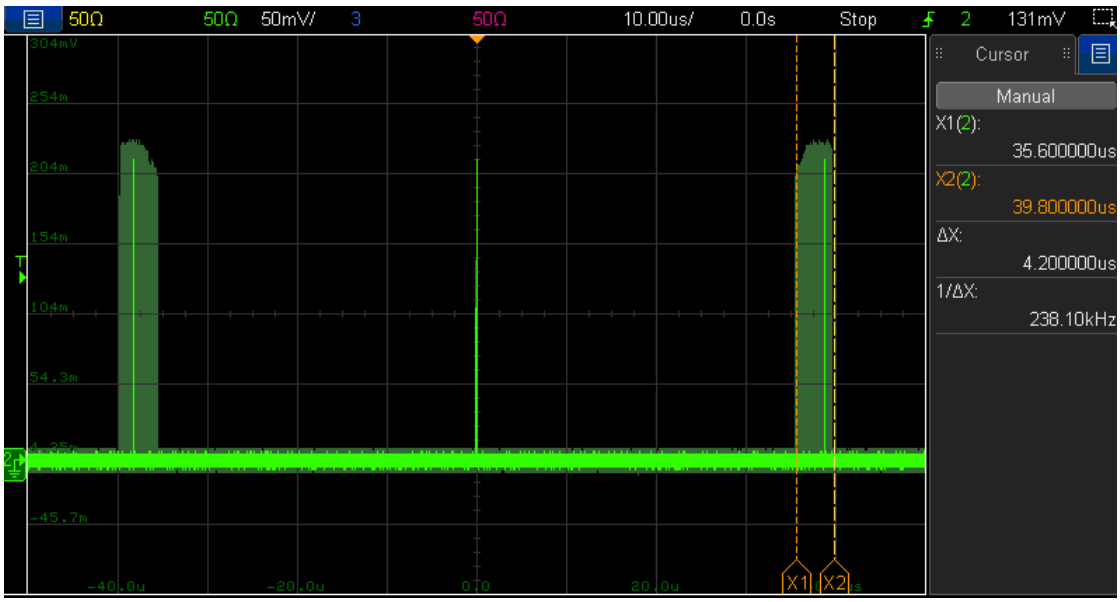

Figure 4.10. *Typical pulse to pulse timing jitter of the 767 nm pulses.*

In the figure above, the pulse repetition rate is rougly 26 kHz. This means that the time between pulses is approximately 38.5 µs. With the timing jitter of 4.2 µs, as shown in figure 4.10, the percentual jitter is around 11 %. This is a rather large timing jitter, mainly due to the reasonably low pulse repetition rate. For comparison, with a pulse repetition rate of 100 kHz, a typical timing jitter is in the range of 200 ns, equaling to about 6 % of the pumping period.

For applications in which the timing jitter or intensity variations are critical parameters, there are several means to reduce their effect. These include for example timing of the pulse generation with an external source or using shorter pump periods with higher intensity. However, for most of the spectroscopy and microscopy applications, as targeted in this work a simple trigger line, to inform of emitted pulses is often sufficient for the start of measurements.

5 CONCLUSIONS

5.1 Main outcomes

This thesis describes the structure and properties of second-harmonic generation of high repetition rate microchip lasers. The development of ns pulsed lasers at 767 nm were targeted as an essential part of the thesis aiming at demonstration of a microchip laser source for novel spectroscopic and microscopic applications. This work included progress on short pulsed SESAM Q-switched microchip seed lasers as well as the nonlinear conversion of these sources to a novel wavelength region.

The targeted specifications included short pulses in the ns regime, high repetition rate from tens to hundreds of kilohertz, short pulse generation with kilowatt pulse peak powers in the early NIR I regime. Studies of different seed laser combinations shooting for these parameters were conducted, showing pulse repetition rates from few kHz all the way to over 800 kHz, all in the ns pulse duration. Out of these sources, second harmonic studies were further conducted, aiming to resolve the best combination of optical parameters both in microscopic wise, as well as for the PPLN frequency doubling.

From the seed laser development, it was noticed that pulse repetition rates of over 40 kHz did not support high enough conversion efficiency to offer sufficient peak powers in the final wavelength and thus the focus was switched to the pulse repetition rates of tens of kHz. This showed promising results, offering conversion efficiencies up to nearly 60 %, and peak powers of over 1 kW. Table 5.1 shows the best output of the 767 nm laser source in tens of kilohertz, representing average power conversion efficiency up to 57.8 %.

Table 5.1. *Frequency converted output to 767 nm.*

Repetition rate (kHz)	Pulse duration (ns)	Peak power (kW)	Conversion efficiency (%)
10	1.2	1.4	52.4
40	1.25	0.83	57.8

It should be however noted, that since the second harmonic generation tends to shorten the pulse duration the peak power conversion efficiency is slightly bit higher than average power conversion efficiency, which is presented in table 5.1. This is in the range of 65.5 % for the 40 kHz laser source, offering some more flexibility for the application use.

Such lasers can be of great use in novel applications such as photoacoustic microscopy.

Microchip lasers have been demonstrated in PAM use multiple times and the combination of short pulses with high repetition rates has shown increase in improving axial resolution of the images. [3] Such lasers require precisely the pulse repetition rate in tens or hundreds of kilohertz with sufficient pulse energy and correct wavelength. Especially the 767 nm wavelength is of interest for the studies of deoxyhemoglobin and hemoglobin separation, in combination with a traditional 532 nm wavelength. This could offer a unique combination of wavelength separation by different absorption levels for different wavelengths.

The medical and academic applications of microchip lasers could include identification of artery from vains, beneath the tissue surface or microscopic imaging ex-vivo. PAM studies have shown that lateral resolution down to 3.8 µm is possible, with such a system utilizing microchip lasers, and the laser properties are essential in the application. Proper emission wavelength is vital for reaching targeted absorption or transmission, depending on the application and the 700 - 800 nm region is extremely useful. For example in the case of hemoglobin, the absorption at 767 nm is very low, whereas at 532 nm there is significant amount of absorption. [36] Thus the use of such lasers together allows for nice separation of different tissues in imaging.

These lasers could have viable placing also in the commercial grounds, as they offer the good optical performance in a compact footprint and affordable cost. The use of SESAM absorbers allows for scalable production and the microchip structure could support efficient production of such devices. The same seed lasers could be utilized in eye-safe LIDAR and ranging applications, due to the good tunability of the optical parameters. Same could be offered to different applications utilizing the nonlinear effect.

Even though the optical development in this thesis aimed at providing a viable laser source for microscopic applications, the same platform could provide laser source for 767 nm sensing. Wavelength range could support Si-based sensing applications, where high pulse repetition rate and short pulses would be highly required. The downside of nonlinear conversion is that compared to the 1534 nm lasers for eye-safe sensing, cost and complexity would be greatly increased. For the microscopic applications this would not be a big issue, as the system requirements on otherparts demand for certain parameters, hard to reach otherwise. For much more price critical sensing, the competing technologies may lack some peak power, but would often beat the microchip solution in size and price.

5.2 Future developments

Demonstration of 767 nm, ns pulsed high repetition rate lasers was a great step in offering a comprehensive and progressible laser solution for novel microscopic applications. However, as seen the results of this thesis, the pulse repetition rate was limited to around 40 kHz due to poor conversion efficiency at higher pulse repetition rates. Considering the application viability of these lasers, this is a significant drawback as the microchip

platform itself can offer repetition rates up to MHz region.

For many applications the need for more accurate sensing correlates to the high number of pulses. This is a clear development step to take for future, enabling use of similar laser platforms at the 767 nm wavelength with repetition rates in the hundreds of kilohertz. The main effects causing this were related to seed laser peak powers, dropping rapidly after 40 kHz and should thus be developed further on to support use of higher repetition rates.

Another development step should focus on bringing the table-top version of these lasers into a more compact casing, naturally encouraged by the microchip structure. The challenges of such development include pushing the nonlinear conversion phase into a chip level process, potentially directly after the microchip itself. These development go however beyond the academic ambition and should be considered taking place in a commercial phase.

REFERENCES

[1] G. Vicidomini, P. Bianchini and A. Diaspro. STED super-resolved microscopy. *Nature methods* 15.3 (2018), 173–182. DOI: https://doi.org/10.1038/nmeth.4593.

[2] T. I. Oy. *Time-Gated Raman spectroscopy*. Accessed on 28.4.2023. URL: https://www.timegate.com/timegated_technology.

[3] G. Nteroli, G. Messa, M. K. Dasa, A. Penttinen, A. Härkönen, M. Guina, A. G. Podoleanu, S. Koutsikou and A. Bradu. Enhanced resolution optoacoustic microscopy using a picosecond high repetition rate Q-switched microchip laser. *Journal of biomedical optics* 27.11 (2022), 110501. DOI: https://doi.org/10.1117/1.JBO.27.11.110501.

[4] M. Ikeda, T. Mizuno, M. Takeya, S. Goto, S. Ikeda, T. Fujimoto, Y. Ohfuji and T. Hashizu. High-power GaN-based semiconductor lasers. *physica status solidi (c)* 1.6 (2004), 1461–1467. DOI: https://doi.org/10.1002/pssc.200304086.

[5] W. Koechner. *Solid-state laser engineering*. Vol. 1. Springer, 2013. ISBN: 978-3-662-15145-7.

[6] P. Wan, L.-M. Yang and J. Liu. High pulse energy 2 μm femtosecond fiber laser. *Optics Express* 21.2 (2013), 1798–1803. DOI: https://doi.org/10.1364/OE.21.001798.

[7] S.-W. Cho, S. M. Park, B. Park, T. G. Lee, B.-M. Kim, C. Kim, J. Kim, S.-W. Lee, C.-S. Kim et al. High-speed photoacoustic microscopy: a review dedicated on light sources. *Photoacoustics* 24 (2021), 100291. DOI: https://doi.org/10.1016/j.pacs.2021.100291.

[8] O. Svelto, D. C. Hanna et al. *Principles of lasers*. Vol. 1. Springer, 2010. ISBN: 978-1-4419-1302-9.

[9] E. Mehner, B. Bernard, H. Giessen, D. Kopf and B. Braun. Sub-20-ps pulses from a passively Q-switched microchip laser at 1 MHz repetition rate. *Optics letters* 39.10 (2014), 2940–2943. DOI: https://doi.org/10.1364/OL.39.002940.

[10] J. Nikkinen. *Sub-100 ps Light Sources Based on Q-Switched Microchip Lasers*. Tampere University of Technology, 2017. ISBN: 978-952-15-4047-9.

[11] E. Räikkönen, O. Kimmelma, M. Kaivola and S. Buchter. Passively Q-switched Nd: YAG/KTA laser at 561 nm. *Optics communications* 281.15-16 (2008), 4088–4091. DOI: https://doi.org/10.1016/j.optcom.2008.04.016.

[12] J. Hellström, G. Karlsson, V. Pasiskevicius, F. Laurell, B. Denker, S. Sverchkov, B. Galagan and L. Ivleva. Passive Q-switching at 1.54 μm of an Er–Yb: GdCa4O (BO3) 3 laser with a CO2+: MgAl2O4 saturable absorber. *Applied Physics B* 81.1 (2005), 49–52. DOI: https://doi.org/10.1007/s00340-005-1832-3.

[13] K. Yumashev, I. Denisov, N. Posnov, P. Prokoshin and V. Mikhailov. Nonlinear absorption properties of Co2+: MgAl2O4 crystal. *Applied Physics B* 70 (2000), 179–184. DOI: https://doi.org/10.1007/s003400050029.

[14] Y. Qi, Z. Bai, Y. Wang, X. Zhang, Y. Qi, J. Ding, Z. Bai and Z. Lu. Research progress of all-solid-state passively Q-switched Er: Yb: glass lasers. *Infrared Physics & Technology* 116 (2021), 103727. DOI: https://doi.org/10.1016/j.infrared.2021.103727.

[15] S. R. Chinn and V. King. Subnanosecond (Er, Yb) Glass Q-Switched Microlasers: 3-D Transient Modeling and Experiments. *IEEE journal of quantum electronics* 42.11 (2006), 1128–1136. DOI: 10.1109/JQE.2006.883470.

[16] B. Denker, B. Galagan, V. Osiko and S. Sverchkov. Active and passive materials for miniature diode-pumped 1.5/spl mu/m erbium glass lasers. *5th International Workshop on Laser and Fiber-Optical Networks Modeling, 2003. Proceedings of LFNM 2003.* IEEE. 2003, 243–244. DOI: 10.1109/LFNM.2003.1246139.

[17] J. Šulc, M. Němec, D. Vyhlıdal, H. Jelınková, K. Nejezchleb and Š. Uxa. Nd: YAG/Cr: YAG microchip-based system for laser-induced damage threshold measurement. *Solid State Lasers XXXII: Technology and Devices*. Vol. 12399. SPIE. 2023, 166–171. DOI: https://doi.org/10.1117/12.2647845.

[18] Y. Honda, S. Motokoshi, T. Jitsuno, N. Miyanaga, K. Fujioka, M. Nakatsuka and M. Yoshida. Temperature dependence of optical properties in Nd/Cr: YAG materials. *Journal of luminescence* 148 (2014), 342–346. DOI: https://doi.org/10.1016/j.jlumin.2013.12.044.

[19] J. J. Zayhowski. Microchip lasers. *Optical materials* 11.2-3 (1999), 255–267. DOI: https://doi.org/10.1016/S0925-3467(98)00048-2.

[20] A. Penttinen. SESAM based Q-Switched microchip lasers. (2020). URL: https://urn.fi/URN:NBN:fi:tuni-202005205501.

[21] A. GmbH. *AlphaLAS PULSELAS P-series*. Accessed on 26.4.2023. URL: https://www.alphalas.com/products/lasers/subnanosecond-passively-q-switched-dpss-microchip-lasers-pulselas-p-series.html/.

[22] C. Inc. *Coherent Revolution*. Accessed on 26.4.2023. URL: https://www.coherent.com/lasers/amplifiers/revolution.

[23] T. Photonics. *Teem Photonics lasers*. Accessed on 26.4.2023. URL: https://www.teemphotonics.com/infrared-green-and-ultraviolet-laser-products/sub-ns-lasers/.

[24] a. B. S. C. Bright Microlaser. *Bright Microlaser*. Accessed on 26.4.2023. URL: https://www.brightmicrolaser.com/.

[25] a. B. S. C. Bright Microlaser. *Bright Microlaser*. Accessed on 26.4.2023. URL: https://www.brightmicrolaser.com/.

[26] A. Penttinen, A. Härkönen and M. Guina. SESAM Q-switched 1534 nm microchip lasers: Pulse duration, repetition rate, and peak-power optimization for LIDAR application. *2019 Conference on Lasers and Electro-Optics Europe & European Quan-*

tum Electronics Conference (CLEO/Europe-EQEC). IEEE. 2019, 1–1. DOI: 10.1109/CLEOE-EQEC.2019.8871709.

[27] R. A. Häring. Miniature pulsed laser sources: repetition rates from kilohertz to gigahertz. PhD thesis. ETH Zurich, 2001. DOI: https://doi.org/10.3929/ethz-a-004276724.

[28] R. Häring, R. Paschotta, R. Fluck, E. Gini, H. Melchior and U. Keller. Passively Q-switched microchip laser at 1.5 μm. *JOSA B* 18.12 (2001), 1805–1812. DOI: https://doi.org/10.1364/JOSAB.18.001805.

[29] R. W. Boyd. *Nonlinear optics*. Academic press, 2020. ISBN: 978-0-323-85057-5.

[30] R. Paschotta. *Article on Quasi Phase Matching*. Accessed on 5th of May, 2023. URL: https://www.rp-photonics.com/quasi_phase_matching.html.

[31] Covesion. *Principles of Nonlinear frequency conversion*. Accessed on 6.5.2023. URL: https://covesion.com/en/resource/principles-of-nonlinear-frequency-conversion/.

[32] J. J. Zayhowski and A. Mooradian. Single-frequency microchip Nd lasers. *Optics letters* 14.1 (1989), 24–26. DOI: https://doi.org/10.1364/OL.14.000024.

[33] C. E. Coatings. *Ion Beam Sputtering coater*. Accessed on 16.5.2023. URL: https://www.cutting-edge-coatings.com//.

[34] M. Polyanskiy. *Refractive Index*. Accessed on 25.4.2023. 2023. URL: https://refractiveindex.info/.

[35] *Device Specification MSHG1550-0.5-xx*. version 5.0. Covesion Inc. 2021. URL: https://covesion.com/en/products/mgoppln-crystals-and-chips/shg-crystals/1550nm-shg-0-5mm/.

[36] W. Zijlstra and A. Buursma. Spectrophotometry of hemoglobin: absorption spectra of bovine oxyhemoglobin, deoxyhemoglobin, carboxyhemoglobin, and methemoglobin. *Comparative Biochemistry and Physiology Part B: Biochemistry and Molecular Biology* 118.4 (1997), 743–749. DOI: https://doi.org/10.1016/S0305-0491(97)00230-7.